

# Explicit error bounds and guaranteed convergence of the Koopman-Hill projection stability method for linear time-periodic dynamics

Fabia Bayer<sup>a,\*</sup>, Remco I. Leine<sup>a</sup>

<sup>a</sup>University of Stuttgart, Institute for Nonlinear Mechanics, Pfaffenwaldring 9, 70569 Stuttgart, Germany

---

## Abstract

The Koopman-Hill projection method is used to approximate the fundamental solution matrix of linear time-periodic ordinary differential equations, possibly stemming from linearization around a periodic solution of a nonlinear dynamical system. By expressing both the true fundamental solution and its approximation as series, we derive an upper bound for the approximation error that decays exponentially with the size of the Hill matrix. Exponential decay of the Fourier coefficients of the system dynamics is key to guarantee convergence. The paper also analyzes a subharmonic formulation that improves the convergence rate. Two numerical examples, including a Duffing oscillator, illustrate the theoretical findings.

*Keywords:* Hill matrix, Floquet multipliers, numerical stability analysis, periodic solutions, monodromy matrix

---

## 1. Introduction

The local stability analysis of periodic solutions of nonlinear dynamical systems described by ordinary differential equations is of prime interest in various fields of engineering and applied mathematics. Periodic solutions arise naturally in many applications, such as structural dynamics [1] and electrical circuits [2]. While only stable periodic solutions can be attained in practical experiments, unstable periodic solutions characterize the global behavior of a system and knowledge of them can be critical to safe operation.

After linearization, the stability properties of a periodic solution are equivalent to those of the origin of a linear time-periodic system (LTP) [3]. Floquet theory provides a powerful framework for analyzing the evolution of LTP systems [4, 5]. In contrast to linear time-invariant systems, the stability is not immediately determined by the spectrum of the system matrix and more sophisticated numerical methods are usually required. Such methods for numerical stability analysis can classically be categorized into two families, with their corresponding operations taking place in the time domain or in the frequency domain, respectively.

The time domain approaches rely on numerical integration to obtain the system's fundamental solution matrix over one period. This yields the monodromy matrix, whose eigenvalues govern the stability. While effective, these methods can be computationally expensive, especially for systems with long periods. The approximation error that these approaches incur is determined by the chosen numerical integration scheme [6, 7]. Global error bounds depending on the local integration error for variable-step integration methods are available for Lipschitz continuous dynamics [7], but are not often explicitly computed in practice. Integration schemes that specifically measure the global error are computationally expensive [8].

Frequency domain methods classically employ a Fourier series representation of the system's solutions. This leads to the formulation of the bi-infinite Hill matrix, which captures the system's dynamics in the frequency domain. Hill stability methods typically involve the full spectral decomposition of a truncated Hill matrix, which is computationally intensive [5, 9, 10]. While there is a guarantee that selected eigenvalues of the truncated Hill matrix do converge to the sought-after Floquet exponents [11], there are no error bounds for any fixed truncation order. These eigenvalues can not be computed directly. Instead, all eigenvalues of the Hill matrix are usually determined first and then the physically meaningful ones are identified using a sorting criterion based on their imaginary part [11]. Other eigenvalue sorting methods showcase better convergence rate numerically [12], but have no convergence guarantee at all.

---

\*Corresponding author

Email addresses: [bayer@inm.uni-stuttgart.de](mailto:bayer@inm.uni-stuttgart.de) (Fabia Bayer), [leine@inm.uni-stuttgart.de](mailto:leine@inm.uni-stuttgart.de) (Remco I. Leine)

The Koopman-Hill projection method, introduced by the authors in 2023 [13], offers a novel approach combining aspects of both frequency and time domain. This method re-interprets the truncated Hill matrix as the system matrix of a time-invariant linear differential equation, allowing for the computation of the fundamental solution matrix using one matrix exponential instead of direct numerical integration. Numerical studies have shown that the Koopman-Hill projection method provides accurate approximations of the monodromy matrix, with the approximation error decreasing as the truncation order of the Hill matrix increases [13–15].

Despite its promising numerical performance, the Koopman-Hill projection method has lacked a theoretical convergence guarantee and rigorous explanation. This paper addresses this gap by providing a convergence proof and explicit closed-form error bounds for the method. The key idea is to express both the true fundamental solution matrix and the Koopman-Hill approximation in a series involving the Fourier coefficients. This series is novel to the authors' knowledge. A term-by-term comparison leads to a bound for the approximation error that decays exponentially with the truncation order of the Hill matrix and depends only on two scalar parameters which govern the decay behavior of the Fourier coefficients of the system matrix.

Previous works of the authors [13, 14] observed that a modified formulation that includes subharmonic frequencies can lead to a significant improvement in the approximation quality of the Koopman-Hill projection. However, these works did not provide an explanation for this improved performance. Using the formalism developed in this paper, we also provide a series expression for this subharmonic formulation and determine its error bound. Compared to the error bound of the direct formulation, this error bound decays at twice the rate, indicating improved accuracy.

The structure of this paper is as follows. Section 2 provides the necessary theoretical background on Floquet theory, the Koopman operator, and the Koopman-Hill projection method, whose convergence properties stand at the center of this work. A scalar example in Section 3 facilitates a first, intuitive understanding of the series expressions that will follow in the later statements.

Sections 4 and 5 are dedicated to proving our main results. At the beginning of Section 4, we state the series expression for the fundamental solution matrix, consisting of scalar factors and products of Fourier coefficient matrices of the time-periodic system matrix. After examining derivative properties of the scalar factor in Section 4.1, we show in Section 4.2 that the series fulfills the underlying LTP differential equation. In Section 4.3, we use analogous arguments to derive a series expression for each  $j$ -shifted Koopman-Hill approximation. In Section 5, a summand-by-summand comparison of the two series expressions reveals the main contribution of this work: A closed-form bound for the approximation error that decays exponentially in the truncation order of the Hill matrix.

Section 6 analyzes the modified, subharmonic formulation for the Koopman-Hill projection and determines its error bound, which decays at twice the rate of the direct formulation. In Section 7, the results of the previous sections are illustrated by numerical examples. Finally, Section 8 concludes the paper with a summary and discussion of the main results and an outlook on future research.

## 2. Theoretical background and notation

This section provides the necessary background for the developments to follow. In particular, we revisit Floquet theory and the Koopman operator. Arguments of [13] are rephrased to motivate the Koopman-Hill projection method for computing the fundamental solution matrix of an LTP system. Further, the multi-index notation that is used throughout the remainder of this paper is introduced.

### 2.1. Floquet Theory

This section revisits some well-known facts from Floquet theory that are the basis for the developments of the following sections. For a more comprehensive treatment of the concepts of this section, the interested reader is referred to [3, 4, 16]. Floquet theory is concerned with the study of LTP dynamical systems of the form

$$\dot{\mathbf{y}}(t) = \mathbf{J}(t)\mathbf{y}(t) , \quad (1)$$

where  $\mathbf{J}(t) = \mathbf{J}(t + T) = \sum_{k \in \mathbb{Z}} \mathbf{J}_k e^{ik\omega t} \in \mathbb{R}^{n \times n}$  is a  $T$ -periodic system matrix that can be described by a Fourier series with the complex-valued Fourier coefficient matrices  $\dots, \mathbf{J}_{-1}, \mathbf{J}_0, \mathbf{J}_1, \dots$ . Dynamical systems of this form are encountered in many applications. For example, parametrically excited mechanical systems such as interacting gears [17] and MEMS devices [18] can intrinsically showcase such LTP dynamics. Periodic

parametric excitation has also been used successfully as a control strategy [19]. However, arguably the main domain of application for Floquet theory is the stability analysis of periodic solutions of nonlinear dynamical systems [3]. Here, the linearized dynamics of a perturbation around a periodic solution are of the above-mentioned form.

Due to the linearity of (1), any initial condition  $\mathbf{y}(t_0)$  is mapped to its solution  $\mathbf{y}(t) = \Phi(t, t_0)\mathbf{y}(t_0)$  by the fundamental solution matrix  $\Phi(t, t_0)$ , which is the unique solution of the matrix initial value problem

$$\dot{\Phi}(t, t_0) = \mathbf{J}(t)\Phi(t, t_0) \quad \Phi(t_0, t_0) = \mathbf{I}. \quad (2)$$

In the literature, any  $n \times n$  matrix that satisfies this differential equation is often referred to as a fundamental solution matrix, regardless of its initial condition. The fundamental solution matrix with the identity initial condition is then specifically termed the *principal* fundamental solution matrix. For brevity, we will refer to this unique matrix with the identity initial condition simply as the fundamental solution matrix. Assuming without loss of generality that  $t_0 = 0$ , we denote the fundamental solution matrix as  $\Phi(t) = \Phi(t, 0)$ .

Floquet's theorem [4] states that the fundamental solution matrix can be expressed as

$$\Phi(t) = \mathbf{P}(t)e^{\mathbf{Q}t}, \quad (3)$$

where  $\mathbf{Q} \in \mathbb{C}^{n \times n}$  is a constant matrix and  $\mathbf{P}(t) = \mathbf{P}(t + T)$  is a  $T$ -periodic complex-values matrix with  $\mathbf{P}(0) = \mathbf{I}$ . The long-term behavior of the solution is only determined by the eigenvalues  $\alpha_1, \dots, \alpha_n$  of  $\mathbf{Q}$ , which are referred to as the Floquet exponents. If all Floquet exponents have a negative real part, the equilibrium at zero (which corresponds to stability of the periodic solution if  $\mathbf{J}(t)$  was obtained that way) is asymptotically stable.

The fundamental solution matrix evaluated after a period,  $\Phi_T := \Phi(T) = e^{\mathbf{Q}T}$ , is called the monodromy matrix. It is of special interest as it provides a discrete mapping of states from one period to the next. If all eigenvalues of the monodromy matrix are inside the unit circle, the solution will always decay from one period to the next, indicating asymptotic stability of the equilibrium at zero. In contrast, if at least one eigenvalue is outside the unit circle, the solution in the corresponding eigendirection will grow from one period to the next, indicating instability. These eigenvalues  $\lambda_1, \dots, \lambda_n$  of the monodromy matrix are called Floquet multipliers and are related to the Floquet exponents by  $\lambda_i = e^{\alpha_i T}$ .

Since the monodromy matrix is usually not available in closed form, numerical methods are needed to approximate the Floquet multipliers. An overview over various methods to obtain the monodromy matrix by numerical integration of (2) can be found in [6]. These numerical integration methods will not be treated further in this work. Alternatively, the periodic nature of the differential equation can be exploited to determine the stability based on the Fourier coefficients of  $\mathbf{J}$ . These so-called Hill methods rely on the Hill matrix, which is given by the Fourier coefficients of the system matrix. While the Hill methods classically consider the full spectral decomposition of the Hill matrix to assert stability [6, 9], the Koopman-Hill projection method [13] computes the monodromy matrix from the Hill matrix using a matrix exponential. This method will be explained in detail in Section 2.3 as it stands in the center of the present work.

## 2.2. The Koopman lift

Compared to LTP systems such as (1), linear autonomous dynamical systems are almost trivial to solve. The crucial idea of the Koopman-Hill projection method, introduced in [13], is to numerically solve the nonautonomous dynamics using an autonomous approximation, at the cost of a larger state space. This is an application of the Koopman framework, in which a nonlinear autonomous system is represented by a linear autonomous system of larger (possibly infinite-dimensional) size.

The Koopman operator was originally introduced for the purpose of extracting global information from nonlinear autonomous dynamics using its spectral decomposition, the so-called Koopman eigenfunctions [20–22]. In recent years, it has been successfully applied in data-driven contexts to generate linear systems that effectively model potentially nonlinear behavior [23–25]. However, for the purpose of deriving the Koopman-Hill approximation, only a matrix representation of the Koopman generator is needed. For the further concepts, the interested reader is referred to the vast Koopman literature (see, e.g., [22] and references therein).

Consider a nonlinear autonomous dynamical system

$$\dot{\mathbf{x}} = \mathbf{f}(\mathbf{x}) \quad (4)$$

in  $\mathbb{R}^n$  with the flow map  $\mathbf{x}(t) = \varphi(t, \mathbf{x}(0))$ . We consider now a space  $\mathcal{F}$  of observable functions  $g : \mathbb{R}^n \rightarrow \mathbb{C}$ . The semigroup of Koopman operators  $\mathcal{K}^t : g \mapsto g \circ \varphi(t, \cdot)$  describes the evolution of these observables along

trajectories of the system [22]. Under the appropriate regularity conditions (cf. [26]), the semigroup is strongly continuous and generated by the infinitesimal Koopman generator

$$\mathcal{L} = \lim_{t \rightarrow 0} \frac{\mathcal{K}^t - \mathbf{I}}{t}, \quad (5)$$

which is given by the Lie derivative of the observable along the flow:

$$(\mathcal{L}g)(\mathbf{x}) = \dot{g}(\mathbf{x}) = \frac{\partial g}{\partial \mathbf{x}} \mathbf{f}(\mathbf{x}). \quad (6)$$

For example, any Lyapunov function  $V$  can be considered as an element of a space of observables, and its derivative  $\dot{V}$ , as needed for Lyapunov's direct method, is given by  $\dot{V} = \mathcal{L}V$ .

The infinitesimal Koopman generator  $\mathcal{L}$  is, by construction, a linear operator on the space of observables, even though the original dynamics are nonlinear. If the original state variables  $g_i(\mathbf{x}) = x_i$  are elements of the function space  $\mathcal{F}$ , the dynamics can be recovered from  $\mathcal{L}$  via (6). Hence, a linear operator can completely describe the evolution of a nonlinear dynamical system. In most cases, however, such a function space that contains the state variables will be infinite-dimensional and unsuitable for direct numerical computations [27].

If the function space  $\mathcal{F}$  is spanned by a countably infinite set of basis functions  $g_1, g_2, \dots$ , a matrix representation of the Koopman generator can be obtained by evaluating (6) explicitly for each basis function. Expressing the result again in terms of the basis functions  $\dot{g}_i = \sum_k a_{ik} g_k$  and collecting all basis functions in a vector  $\mathbf{z}^T = (g_1, g_2, \dots)$  then yields

$$\dot{\mathbf{z}} = \mathbf{A} \mathbf{z}. \quad (7)$$

We call  $\mathbf{z}$  the lifted state vector. Consider now a *consistent* initial condition, such that  $\mathbf{z}_0^T = (g_1(\mathbf{x}_0), g_2(\mathbf{x}_0), \dots)$  is obtained by evaluating all basis functions at the same state-space point  $\mathbf{x}_0$ . Then, the solution of (7) at time  $t$ , given by  $\mathbf{z}(t) = e^{\mathbf{A}t} \mathbf{z}_0$ , contains the values of the basis functions evaluated at  $\mathbf{x}(t) = \varphi(t, \mathbf{x}_0)$ . With a suitable, potentially nonlinear map  $\mathbf{C}(\mathbf{z})$  that fulfills  $\mathbf{x} = \mathbf{C}(\mathbf{g}(\mathbf{x}))$  and projects the lifted states back to the original state space, any point  $\mathbf{x}(t)$  on the trajectory of the original, nonlinear dynamics can be exactly determined using

$$\mathbf{x}(t) = \mathbf{C}(\mathbf{z}(t)) = \mathbf{C}(e^{\mathbf{A}t} \mathbf{g}(\mathbf{x}_0)). \quad (8)$$

In words, as long as  $e^{\mathbf{A}t}$  is a well-defined and bounded operator, any trajectory of the original nonlinear dynamics can be exactly determined by considering the corresponding lifted initial condition, evolving the linear (but infinite-dimensional) lifted system and mapping the result back to the original state space.

In practice, the infinite-dimensional lifted system is truncated to a finite-dimensional system by considering only a finite number  $g_1, \dots, g_M$  of basis functions such that  $\mathbf{A}$  becomes a finite-dimensional matrix. Obviously, this introduces a truncation error into (8). Depending on the chosen function space, this truncation error does not necessarily become small as  $M$  increases. Nonetheless, especially in data-driven contexts, the truncated lifted dynamics have been applied with great success to analyze and control the dynamics of nonlinear systems [23, 24, 28, 29]. The Koopman-Hill projection method to approximate the fundamental solution matrix of a linear time-periodic system follows from these ideas as a special case. This construction is showcased in the next section.

### 2.3. Koopman-Hill projection

In this section, we will repeat and slightly rephrase the arguments of [13] to show how the Koopman-Hill projection method results as a special case from the Koopman lift that was introduced in the previous section. The Koopman lift as introduced above is valid for nonlinear autonomous dynamical systems of the form (4). However, the underlying dynamical system (1) for the Koopman-Hill projection is a linear nonautonomous time-periodic system with period  $T$  and angular frequency  $\omega$ . To bring this system into the required form, we use the extended state space dynamics

$$\dot{t} = 1 \quad (9a)$$

$$\dot{\mathbf{y}} = \mathbf{J}(t) \mathbf{y} \quad (9b)$$

with the extended state space  $\mathbf{x}^T = (t, \mathbf{y}^T)$ . As infinite-dimensional function space  $\mathcal{F}$  we choose the space spanned by the complex-valued basis functions

$$g_{k,i}(t, \mathbf{y}) = y_l e^{-ik\omega t} \quad (10)$$

with  $k \in \mathbb{Z}$  and  $l \in \{1, \dots, n\}$ . The bi-infinite vector that collects all basis functions is

$$\mathbf{g}(t, \mathbf{y}) = \begin{pmatrix} \vdots \\ \mathbf{y}e^{i\omega t} \\ \mathbf{y} \\ \mathbf{y}e^{-i\omega t} \\ \vdots \end{pmatrix}, \quad (11)$$

i.e., the Kronecker product of the original state  $\mathbf{y}$  with the Fourier basis functions in *descending* order.

To determine the Koopman lift according to Section 2.2, we need to evaluate the Lie derivative of the basis functions along the flow of the extended state space dynamics. Expressing the system matrix  $\mathbf{J}(t)$  in terms of its Fourier coefficients, we obtain for the  $k$ -th block of basis functions by the product rule

$$\dot{\mathbf{g}}_k = \frac{d}{dt}(\mathbf{y}e^{-ik\omega t}) = \dot{\mathbf{y}}e^{-ik\omega t} - ik\omega \mathbf{y}e^{-ik\omega t} = (-ik\omega \mathbf{I} + \sum_{l \in \mathbb{Z}} \mathbf{J}_l e^{il\omega t})e^{-ik\omega t} \mathbf{y} = -ik\omega \mathbf{g}_k + \sum_{\tilde{l} \in \mathbb{Z}} \mathbf{J}_{k-\tilde{l}} \mathbf{g}_{\tilde{l}}. \quad (12)$$

The index shift  $\tilde{l} = k - l$  has been used in the last step. Collecting (12) for all values of  $k$  yields the bi-infinite matrix expression

$$\dot{\mathbf{g}} = \begin{pmatrix} \ddots & & & & & & \\ \dots & \mathbf{J}_0 + i\omega \mathbf{I} & \mathbf{J}_{-1} & \mathbf{J}_{-2} & \dots & & \\ \dots & \mathbf{J}_1 & \mathbf{J}_0 & \mathbf{J}_{-1} & \dots & & \\ \dots & \mathbf{J}_2 & \mathbf{J}_1 & \mathbf{J}_0 - i\omega \mathbf{I} & \dots & & \\ & & & & & \ddots & \end{pmatrix} \mathbf{g} =: \mathbf{H}_\infty \mathbf{g}. \quad (13)$$

This is a Koopman lift of the form (7) with the bi-infinite matrix  $\mathbf{H}_\infty$  being the matrix representation of the infinitesimal Koopman generator. The matrix  $\mathbf{H}_\infty$ , constructed from the Fourier coefficients of  $\mathbf{J}(t)$  in this fashion, is well-known as the infinite Hill matrix of the LTP system (1) [5,9]. Its point spectrum is constituted of the Floquet exponents of the system, while its continuous and residual spectrum are either empty or contain only  $\{\infty\}$  [11].

As we assumed  $t_0 = 0$  without loss of generality, the exponential term drops out in

$$\mathbf{g}_k(0, \mathbf{y}_0) = \mathbf{y}_0 e^{-0ik\omega} = \mathbf{y}_0 \quad (14)$$

for all  $k \in \mathbb{Z}$ , and thus any consistent initial condition  $\mathbf{z}_0 = \mathbf{g}(0, \mathbf{y}_0) = (\dots, \mathbf{y}_0^T, \mathbf{y}_0^T, \dots)^T =: \mathbf{W}_\infty \mathbf{y}_0$  of the lifted state is given by a bi-infinite stack of the corresponding original initial condition  $\mathbf{y}_0$ . We denote the linear map that maps a vector  $\mathbf{y}_0$  to a bi-infinite stack of itself by  $\mathbf{W}_\infty$ . Similarly, one possible projection  $\mathbf{C}(t, \mathbf{y})$  that projects the lifted states back to the original state space is given by the linear map  $\mathbf{C}_\infty$ , where  $\mathbf{C}_\infty \mathbf{g}(t, \mathbf{y})$  simply returns the centermost entry  $\mathbf{g}_0(t, \mathbf{y}) = \mathbf{y}$ . Hence, with (8), states  $\mathbf{y}(t)$  on the trajectory of (1) are given by

$$\mathbf{y}(t) = \mathbf{C}_\infty e^{\mathbf{H}_\infty t} \mathbf{W}_\infty \mathbf{y}_0. \quad (15)$$

The bi-infinite matrix product  $\mathbf{C}_\infty e^{\mathbf{H}_\infty t} \mathbf{W}_\infty$  maps arbitrary initial conditions  $\mathbf{y}_0$  to their solution at time  $t$ . This means that this is an expression of the fundamental solution matrix. In particular, evaluated at  $t = T$ , this expression gives the monodromy matrix

$$\Phi_T = \mathbf{C}_\infty e^{\mathbf{H}_\infty T} \mathbf{W}_\infty. \quad (16)$$

As no truncations have happened yet, (16) is exact if  $e^{\mathbf{H}_\infty T} \mathbf{W}_\infty$  yields a bounded result. Conditions for the boundedness of  $\mathbf{H}_\infty$  are discussed in [11].

In practice, the bi-infinite matrix is truncated to the finite-dimensional Hill matrix  $\mathbf{H} \in \mathbb{C}^{n(2N+1) \times n(2N+1)}$  of truncation order  $N$  by considering only the  $2N+1$  centermost row and column blocks of  $\mathbf{H}_\infty$ . The projection matrices  $\mathbf{W}_\infty$  and  $\mathbf{C}_\infty$  are then truncated accordingly to yield

$$\Phi_T \approx \mathbf{C} e^{\mathbf{H} T} \mathbf{W} \quad (17a)$$

$$\mathbf{C} = (\mathbf{0} \quad \dots \quad \mathbf{0} \quad \mathbf{I} \quad \mathbf{0} \quad \dots \quad \mathbf{0}) \quad (17b)$$

$$\mathbf{W} = (\mathbf{I} \quad \dots \quad \mathbf{I})^T. \quad (17c)$$

While the boundedness of  $e^{\mathbf{HT}} \mathbf{W}$  is always given in the finite domain, the introduction of a truncation error must now be considered. Previous numerical studies have indicated that the error between the right-hand side and the left-hand side of (17a) decreases as the truncation order  $N$  increases [13–15]. The central objective of this work is to provide theoretical support for these numerical findings by constructing a bound for the error between both sides of (17a) and demonstrating that this bound decays exponentially as  $N$  increases.

#### 2.4. Multi-index notation

For the sake of brevity, we introduce here two different types of index notation, which are used throughout this work. The natural numbers  $\mathbb{N}$  always include zero. We denote 1-norms by  $|\cdot|$  (with one vertical bar), even for tuples with more than one entry. By  $\|\cdot\|$  (with two vertical bars) we denote an arbitrary vector  $p$ -norm and its induced matrix norm.

**Definition 1** (Multi-index). A tuple  $\boldsymbol{\alpha} \in \mathbb{N}^m$  of  $m$  nonnegative integers is called *multi-index* (in the classical sense). The multi-index has a 1-norm

$$|\boldsymbol{\alpha}| := \sum_{k=1}^m \alpha_k \quad (18)$$

given by the sum of its entries. For a vector  $\mathbf{x} \in \mathbb{C}^m$ , we denote by

$$\mathbf{x}^{\boldsymbol{\alpha}} := \prod_{k=1}^m x_k^{\alpha_k} \quad (19)$$

monomials in  $\mathbf{x}$  of degree  $|\boldsymbol{\alpha}|$ . We define  $0^0 := 1$  to avoid restricting the values that  $\mathbf{x}$  may admit.

*Example 2.1.* The multi-index  $\boldsymbol{\alpha} = [2, 0, 1, 0]$  has norm  $|\boldsymbol{\alpha}| = 3$  and  $\mathbf{x}^{\boldsymbol{\alpha}} = x_1^2 x_3$  for all  $\mathbf{x} = [x_1, x_2, x_3, x_4] \in \mathbb{C}^4$ .

**Definition 2** (Integer index tuples and products of Fourier coefficients). A tuple  $\mathbf{p} \in \mathbb{Z}^m$  of  $m$  integers is called an *integer index tuple*. It has a 1-norm

$$|\mathbf{p}| := \sum_{k=1}^m |p_k|, \quad (20)$$

which is generally not equal to the sum of its entries. Any integer index tuple  $\mathbf{p} \in \mathbb{Z}^m$  uniquely describes an (ordered) *product of  $m$  Fourier coefficient matrices*

$$\mathcal{J}_{\mathbf{p}} := \prod_{k=1}^m \mathbf{J}_{p_k} = \mathbf{J}_{p_1} \mathbf{J}_{p_2} \cdots \mathbf{J}_{p_m}. \quad (21)$$

The ordering of the entries of  $\mathbf{p}$  is important as the matrices  $\mathbf{J}_k$  generally do not commute.

*Example 2.2.* Consider as an example the integer index tuple  $\mathbf{p} = [-3, 0, 1, 1]$ , which defines uniquely the product of Fourier coefficients

$$\mathcal{J}_{[-3,0,1,1]} = \mathbf{J}_{-3} \mathbf{J}_0 \mathbf{J}_1 \mathbf{J}_1 = \mathbf{J}_{-3} \mathbf{J}_0 \mathbf{J}_1^2.$$

As  $\mathbb{Z}^m$  is a subset of  $\mathbb{C}^m$ , integer index tuples can be exponentiated by multi-indices using (19). With  $\boldsymbol{\alpha} = [2, 0, 1, 0]$  and  $\mathbf{p} = [-3, 0, 1, 1]$  as before, we obtain

$$\mathbf{p}^{\boldsymbol{\alpha}} = [-3, 0, 1, 1]^{[2,0,1,0]} = (-3)^2 \cdot 0^0 \cdot 1^1 \cdot 1^0 = 9$$

and even

$$\mathbf{p}^{\boldsymbol{\alpha}} \mathcal{J}_{\mathbf{p}} = 9 \mathbf{J}_{-3} \mathbf{J}_0 \mathbf{J}_1^2.$$

*Example 2.3.* For an integer index tuple  $\mathbf{p} = [p_1, \dots, p_m] \in \mathbb{Z}^m$  and a multi-index  $\boldsymbol{\alpha} = [\alpha_1, \dots, \alpha_m] \in \mathbb{N}^m$ , a specific multi-index expression that will become important later is

$$[p_1, p_1 + p_2, \dots, p_1 + \dots + p_m]^{\boldsymbol{\alpha}} = \prod_{k=1}^m \left( \sum_{l=1}^k p_l \right)^{\alpha_k} = p_1^{\alpha_1} (p_1 + p_2)^{\alpha_2} \cdots (p_1 + \dots + p_m)^{\alpha_m}, \quad (22)$$

consisting of a product of  $m$  factors, where the  $k$ -th factor is given by the sum of the first  $k$  entries of the integer index tuple, exponentiated by  $\alpha_k$ .

### 3. Scalar example

Before delving into the full generality of the main statements, this section is dedicated to a scalar example, which illustrates the series expression that is key throughout this paper.

*Example 3.1.* Consider the scalar LTP dynamics

$$\dot{y} = J(t)y = (\beta + 2\gamma \cos t)y \quad (23)$$

with  $\beta, \gamma \in \mathbb{R}$ . The Fourier coefficients of the system matrix  $J(t)$  (here scalar) can be immediately read off:  $J_0 = \beta$ ,  $J_1 = J_{-1} = \gamma$ . All other Fourier coefficients are zero. As the differential equation is scalar and linear, solutions are available in closed form. In particular, the fundamental solution matrix (here scalar), i.e., the solution initialized at  $y(0) = 1$ , is given by

$$\phi(t, \beta, \gamma) = e^{(\beta t + 2\gamma \sin t)} . \quad (24)$$

To study the influence of the Fourier coefficients on the solution, one may seek to express the fundamental solution as a Taylor series in  $\beta, \gamma$  with arbitrary but fixed  $t$ . That is, dependencies on  $t$  are allowed to appear within arbitrary nonlinearities, while dependencies on  $\beta$  and  $\gamma$  may only appear polynomially. The Taylor series coefficients are given by the derivatives with respect to  $\beta$  and  $\gamma$ . As both  $\beta$  and  $\gamma$  appear linearly inside the exponential of (24), these derivatives are

$$\frac{\partial^{(l+k)}}{\partial \beta^l \partial \gamma^k} \phi(t, \beta, \gamma) = t^l (2 \sin t)^k e^{(\beta t + 2\gamma \sin t)} . \quad (25)$$

Evaluated at  $\beta = \gamma = 0$ , the exponential term becomes 1. Hence, the Taylor series of the fundamental solution with respect to its Fourier coefficients is given by

$$\phi(t, \beta, \gamma) = \sum_{l=0}^{\infty} \sum_{k=0}^{\infty} \frac{t^l (2 \sin t)^k}{(l+k)!} \beta^l \gamma^k =: \sum_{l,k \in \mathbb{N}} \hat{\xi}(l, k, t) \beta^l \gamma^k . \quad (26)$$

This series form is a scalar variant of the general series expressions that will be derived for the fundamental solution matrix and its Koopman-Hill approximation in the following sections. Specifically, the monomials  $\beta^l \gamma^k$  of Fourier coefficients are weighted by a scalar function  $\hat{\xi}(l, k, t)$ , which depends nonlinearly on the time  $t$  and the degree  $(l, k)$  of the monomial. In particular,  $\hat{\xi}(l, k, t)$  consists of a polynomial in  $t$  modulated by a periodic function. These properties will also be present in the general series expressions derived later.

As a next step, we bring the direct Koopman-Hill projection approximation into a form that is structurally similar to (26). A comparison with the general Hill matrix structure (13) reveals that the Hill matrix of (24) with truncation order  $N$  is given by

$$\mathbf{H}(\beta, \gamma) := -i\mathbf{D} + \beta\mathbf{I} + \gamma\mathbf{R} , \quad (27)$$

where  $\mathbf{D} = \text{diag}(-N, \dots, N)$  is diagonal and independent of the Fourier coefficients, and  $\mathbf{R}$  is a matrix which has ones on its first sub- and superdiagonal and zeros everywhere else. To express the Koopman-Hill approximation

$$\phi_{\text{approx}}(t, \beta, \gamma) = \mathbf{C} e^{\mathbf{H}(\beta, \gamma)t} \mathbf{W} =: \sum_{l,k \in \mathbb{N}} \hat{\xi}_{\text{approx}}(l, k, t) \beta^l \gamma^k \quad (28)$$

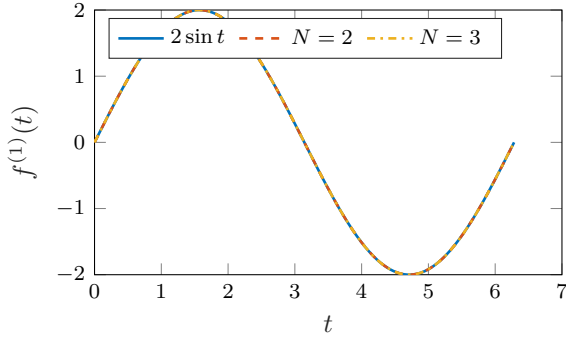
as a Taylor series that is structurally the same as (26), again the partial derivatives with respect to  $\beta$  and  $\gamma$  are needed. The decomposition of  $\mathbf{H}$  into the three summands allows to write

$$e^{\mathbf{H}(\beta, \gamma)t} = e^{\beta t} e^{(-i\mathbf{D} + \gamma\mathbf{R})t} \quad (29)$$

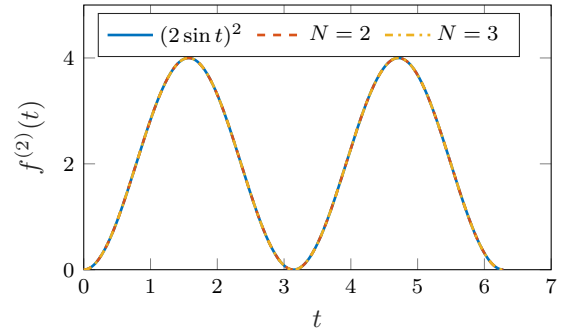
and therefore the partial derivative w.r.t  $\beta$  is simply

$$\frac{\partial^l}{\partial \beta^l} e^{\beta t} \mathbf{C} e^{(-i\mathbf{D} + \gamma\mathbf{R})t} \mathbf{W} = t^l e^{\beta t} \mathbf{C} e^{(-i\mathbf{D} + \gamma\mathbf{R})t} \mathbf{W} . \quad (30)$$

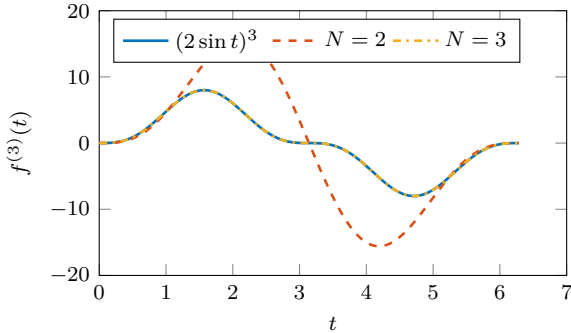
Evaluated at  $\beta = \gamma = 0$ , as  $\mathbf{C}\mathbf{D} = \mathbf{0}$ , the exponential terms again become 1 and only  $t^l$  remains. This results in identical summands in the Taylor series (28) and (26) for  $k = 0$ . For  $k > 0$ , also the partial derivative w.r.t



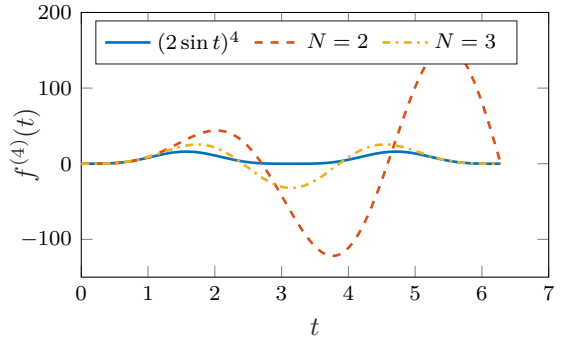
(a) Right-hand side and left-hand side of (31) for  $k = 1$ .



(b) Right-hand side and left-hand side of (31) for  $k = 2$ .



(c) Right-hand side and left-hand side of (31) for  $k = 3$ .



(d) Right-hand side and left-hand side of (31) for  $k = 4$ .

Figure 1: Right-hand side (blue, solid) and left-hand side of (31) (orange, dashed – truncation order  $N = 2$ ; yellow, dashdotted – truncation order  $N = 3$ ) for  $k = 1, 2, 3, 4$ .

$\gamma$  is needed. Unfortunately, this partial derivative w.r.t  $\gamma$  is not easily expressed in closed form since  $\mathbf{D}$  and  $\mathbf{R}$  do not commute.

If there was no approximation error, we would expect that the partial derivatives with respect to  $\gamma$  are given by

$$\left. \frac{\partial^k}{\partial \gamma^k} \mathbf{C} e^{(-i\mathbf{D} + \gamma \mathbf{R})t} \mathbf{W} \right|_{\gamma=0} \stackrel{!}{=} (2 \sin t)^k. \quad (31)$$

However, due to the error from the truncation, this equality will not hold exactly for all  $k$ . The functions on the left-hand side and on the right-hand side of (31) are depicted in Figure 1 for truncation orders  $N = 2$  and  $N = 3$  and  $k = 1, 2, 3, 4$ . Hereby, the partial derivatives were evaluated numerically using Cauchy's integral formula [30] with the trapezoid rule. Figure 1 shows that the right-hand side of (31) is well approximated by the left-hand side if  $k \leq N$ . For  $k > N$ , the derivatives of the true fundamental solution and its Koopman-Hill approximation do not match. However, higher derivatives are divided by  $(l + k)!$  in (26) and (28), which suggests that the approximation error incurred for a certain  $k$  is small if  $k$  is large. In particular, we expect the approximation error to converge to zero as  $N$  increases, and with it the number of summands that are exactly met.

To summarize, the scalar example showcases the following crucial properties:

- Both the fundamental solution and the Koopman-Hill approximation can be expressed as a series of monomials in the Fourier coefficients, each multiplied by a scalar factor.
- The scalar factor is independent of the Fourier coefficients and can consist of polynomial and periodic components in  $t$ .
- For monomials whose degree is bounded by the truncation order  $N$  of the Hill matrix, the scalar factor of the Koopman-Hill approximation matches exactly the corresponding factor of the true fundamental solution. The approximation error occurs only in the higher degrees.



#### 4. A series representation for the fundamental solution matrix and its approximation

In this section, we state and prove the first contribution of this work: An infinite series representation of the fundamental solution matrix of LTP dynamics, which is novel to the knowledge of the authors. The overall purpose of the present section is to formulate a series expression similar to (26), which organizes the fundamental solution matrix of (1) into a series of time-dependent terms multiplied with products of the Fourier coefficients. To ensure absolute convergence of this expression, we need the following assumption.

**Assumption 1.** There are constants  $a, b > 0$  and a matrix  $p$ -norm  $\|\cdot\|$  such that the Fourier coefficient matrices of  $\mathbf{J}(t)$  in (1) decay exponentially with

$$\|\mathbf{J}_k\| \leq ae^{-b|k|} \quad \text{for all } k \in \mathbb{Z}. \quad (32)$$

By the Paley-Wiener theorem, this assumption holds if  $\mathbf{J}(t)$  is analytic [31, Lemma 5.6]. In the context of stability of periodic solutions of nonlinear dynamics, analyticity of the differential equation in all its arguments is sufficient to guarantee analyticity of the solution and thus analyticity of  $\mathbf{J}(t)$  [4, Thm 4.1]. In particular, if the Fourier coefficients of  $\mathbf{J}(t)$  have finite support, then Assumption 1 is satisfied for any fixed  $b > 0$  with  $a = \max_k \|\mathbf{J}_k\| e^{b|k|}$ . Under Assumption 1, the norm of the product of Fourier coefficients  $\mathcal{J}_{\mathbf{p}}$  as defined in (21) can be easily bounded as well:

$$\|\mathcal{J}_{\mathbf{p}}\| \leq \|\mathbf{J}_{p_1}\| \dots \|\mathbf{J}_{p_m}\| \leq a^m e^{-b|\mathbf{p}|}. \quad (33)$$

Here, the matrix  $p$ -norm of the Fourier coefficient matrices reduces to a 1-norm in the integer index tuple  $\mathbf{p}$ .

We are now ready to formulate our first result about a series representation of the fundamental solution matrix. This theorem also contains the definition of the scalar factor.

**Theorem 1** (Series formulation of  $\Phi(t)$ ). *If the Fourier coefficient matrices of (1) fulfill Assumption 1, then the fundamental solution matrix is given by the absolutely convergent series*

$$\Phi(t) = \mathbf{I} + \sum_{m=1}^{\infty} \sum_{\mathbf{p} \in \mathbb{Z}^m} \xi_{\mathbf{p}}(t) \mathcal{J}_{\mathbf{p}} \quad (34)$$

with the scalar, complex-valued factor

$$\xi_{\mathbf{p}}(t) := \sum_{\boldsymbol{\alpha} \in \mathbb{N}^m} \frac{t^{m+|\boldsymbol{\alpha}|}}{(m+|\boldsymbol{\alpha}|)!} (i\omega)^{|\boldsymbol{\alpha}|} [p_1, p_1 + p_2, \dots, p_1 + \dots + p_m]^{\boldsymbol{\alpha}} \quad (35)$$

that is independent of the specific dynamical system.

Similarly as in the example (26), the fundamental solution is expressed in terms of (now ordered) monomials of Fourier coefficients, with each such monomial multiplied by a scalar factor  $\xi_{\mathbf{p}}(t)$  that only depends on the time  $t$  and the degree  $\mathbf{p}$  of the monomial. Before proving Theorem 1 in Section 4.2 by showing that (34) satisfies the differential equation (2), the following subsection will analyze the scalar factor  $\xi_{\mathbf{p}}(t)$  in more detail.

##### 4.1. Scalar factor $\xi_{\mathbf{p}}(t)$

As a preliminary step for the analysis of the series expression (34), useful properties of the scalar factor  $\xi_{\mathbf{p}}(t)$  are established in this section. Figure 2 shows the real and imaginary parts of  $\xi_{\mathbf{p}}(t)$  over three periods ( $\omega = 1$ ) for three exemplary values of  $\mathbf{p}$ . Like in the example of Section 3, all these examples grow at most polynomially and exhibit oscillatory behavior. The values of  $\xi_{\mathbf{p}}(t)$  may be complex-valued, with real part and imaginary part oscillating with the same frequency, but potentially very different magnitudes. The following lemma provides a polynomial bound on the absolute value of the scalar factor.

**Lemma 2** (Bound of  $\xi_{\mathbf{p}}(t)$ ). *For all  $m \in \mathbb{N} \setminus \{0\}$ ,  $\mathbf{p} \in \mathbb{Z}^m$ , and  $t \in \mathbb{R}$ , the series (35) over all multi-indices of length  $m$  is absolutely convergent and bounded by*

$$|\xi_{\mathbf{p}}(t)| \leq \frac{|t|^m}{m!}. \quad (36)$$

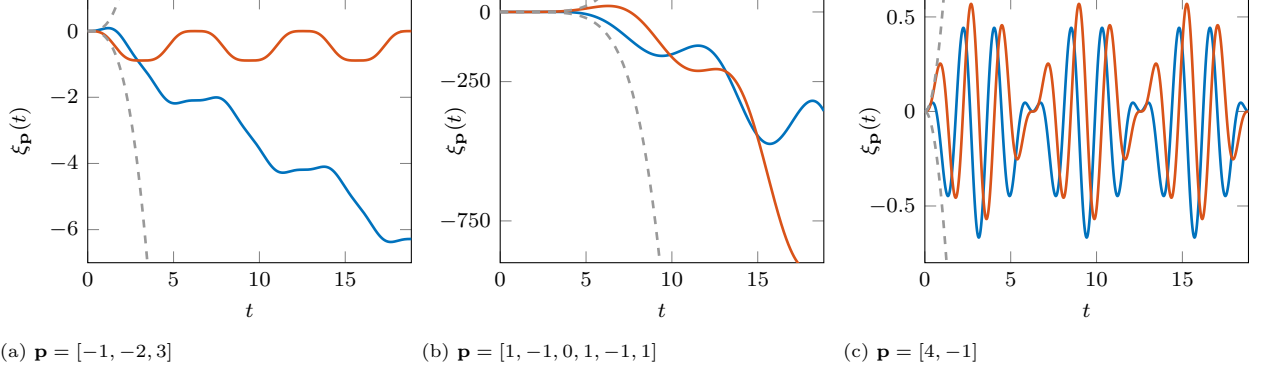


Figure 2: Real part (blue), imaginary part (orange), and polynomial upper bound (36) (grey, dashed) of the scalar factor  $\xi_{\mathbf{p}}(t)$  over three periods for three exemplary values of  $\mathbf{p}$ . Data was computed using Lemma 3 and numerical quadrature with trapezoidal rule.

*Proof.* First we establish absolute convergence. Using for all  $k = 1, \dots, m$  the bound

$$(p_1 + \dots + p_k)^{\alpha_k} \leq (|p_1| + \dots + |p_k|)^{\alpha_k} \leq (|p_1| + \dots + |p_k| + \dots + |p_m|)^{\alpha_k} = |\mathbf{p}|^{\alpha_k}, \quad (37)$$

the multi-index expression is bounded by

$$[p_1, p_1 + p_2, \dots, p_1 + \dots + p_m]^{\alpha} \leq |\mathbf{p}|^{(\alpha_1 + \dots + \alpha_m)} = |\mathbf{p}|^{|\alpha|}. \quad (38)$$

We denote summands of (35) by

$$s_{\alpha} := \frac{t^{m+|\alpha|}}{(m+|\alpha|)!} (i\omega)^{|\alpha|} [p_1, p_1 + p_2, \dots, p_1 + \dots + p_m]^{\alpha}. \quad (39)$$

With (38), the summands are bounded via

$$|s_{\alpha}| \leq \frac{|t|^{m+|\alpha|}}{(m+|\alpha|)!} \omega^{|\alpha|} |\mathbf{p}|^{|\alpha|}. \quad (40)$$

As the right-hand side only depends on the 1-norm  $|\alpha|$  and not on the actual value of  $\alpha$  itself, the sum over all  $\alpha \in \mathbb{N}^m$  can be expressed by a sum over all norms  $M := |\alpha| \in \mathbb{N}$ , where we count for each  $M$  the number of tuples  $\alpha \in \mathbb{N}^m$  with that norm. Using Lemma 10i) from Appendix A, there are exactly  $\binom{M+m-1}{m-1}$  such tuples for a given norm  $M$ . This simplifies (40) to

$$\sum_{\alpha \in \mathbb{N}^m} |s_{\alpha}| \leq \sum_{M=0}^{\infty} \sum_{\substack{\alpha \in \mathbb{N}^m \\ |\alpha|=M}} \frac{|t|^{m+M}}{(m+M)!} \omega^M |\mathbf{p}|^M \quad (41)$$

$$= \sum_{M=0}^{\infty} \frac{(M+m-1)!}{M!(m-1)!} \frac{|t|^{m+M}}{(m+M)(m+M-1)!} \omega^M |\mathbf{p}|^M \quad (42)$$

$$= \sum_{M=0}^{\infty} \frac{|t|^m}{(m-1)!(m+M)} \frac{(|\mathbf{p}| |\omega t|)^M}{M!}. \quad (43)$$

After using  $(m+M) \geq m$  to pull out the first factor, and identifying the exponential series in the second factor, the bound

$$\sum_{\alpha \in \mathbb{N}^m} |s_{\alpha}| \leq \frac{|t|^m}{m!} e^{|\mathbf{p}| |\omega t|} < \infty \quad (44)$$

follows. Now that absolute convergence is established, we derive the tighter bound (36) by considering the

actual values  $s_\alpha$  instead of their magnitudes. Using  $(m + |\alpha|)! \geq (m! \alpha_1! \dots \alpha_m!)$ , we can bound

$$\begin{aligned} |\xi_{\mathbf{p}}(t)| &\leq \left| \sum_{\alpha \in \mathbb{N}^m} \frac{t^{m+|\alpha|}}{m! \alpha_1! \dots \alpha_m!} (i\omega)^{|\alpha|} [p_1, p_1 + p_2, \dots, p_1 + \dots + p_m]^\alpha \right| \\ &= \left| \frac{t^m}{m!} \left( \sum_{\alpha_1=0}^{\infty} \frac{(i\omega p_1 t)^{\alpha_1}}{\alpha_1!} \right) \left( \sum_{\alpha_2=0}^{\infty} \frac{(i\omega(p_1 + p_2)t)^{\alpha_2}}{\alpha_2!} \right) \dots \left( \sum_{\alpha_m=0}^{\infty} \frac{(i\omega(p_1 + \dots + p_m)t)^{\alpha_m}}{\alpha_m!} \right) \right|. \end{aligned} \quad (45)$$

where the sums were reorganized in the second step into factors that each only depend on one  $\alpha_k$ . In every round bracket of (45), the power series of the exponential function can be identified. This simplifies the expression to

$$|\xi_{\mathbf{p}}(t)| \leq \left| \frac{t^m}{m!} e^{i\omega p_1 t} e^{i\omega(p_1+p_2)t} \dots e^{i\omega(p_1+\dots+p_m)t} \right| = \frac{|t|^m}{m!}. \quad (46)$$

□

The series expression for  $\xi_{\mathbf{p}}(t)$  can also be differentiated summand by summand. After some reorganization, this leads to a recursive differential relationship between the scalar factors for various lengths of  $\mathbf{p}$ , covered in the following lemma.

**Lemma 3** (Derivative of  $\xi_{\mathbf{p}}(t)$ ). *The derivative of  $\xi_{\mathbf{p}}(t)$  fulfills the following relations:*

- 1) For  $m = 1$ ,  $p \in \mathbb{Z}$  it holds that  $\dot{\xi}_p(t) = e^{ip\omega t}$ .
- 2) For  $m > 1$ ,  $\mathbf{p} = [p_1, \dots, p_m] \in \mathbb{Z}^m$  it holds that  $\dot{\xi}_{\mathbf{p}}(t) = \xi_{[p_2, \dots, p_m]}(t) e^{ip_1\omega t}$ .

*Proof.* For  $m = 1$ , the derivative of (35) becomes

$$\dot{\xi}_p(t) = \frac{d}{dt} \left( \sum_{\alpha \in \mathbb{N}} \frac{t^{\alpha+1}}{(\alpha+1)!} (i\omega p)^\alpha \right) = \sum_{\alpha=0}^{\infty} \frac{t^\alpha}{\alpha!} (i\omega p)^\alpha = e^{ip\omega t}, \quad (47)$$

For  $m \geq 2$ , consider a fixed  $\mathbf{p} \in \mathbb{Z}^m$ . We define partial sums of  $\mathbf{p}$ , excluding  $p_1$ , by  $b_k := \sum_{l=2}^k p_l$  for all  $k = 2, \dots, m$ . With the power series expression for the exponential  $e^{ip_1\omega t} = \sum_{\alpha_1=0}^{\infty} \frac{(ip_1\omega t)^{\alpha_1}}{\alpha_1!}$  and the explicit expression for  $\xi_{[p_2, \dots, p_m]}$  of (35), the right-hand side becomes

$$\xi_{[p_2, \dots, p_m]}(t) e^{ip_1\omega t} = \sum_{\alpha_1=0}^{\infty} \sum_{[\alpha_2, \dots, \alpha_m] \in \mathbb{N}^{m-1}} \frac{t^{m-1} (i\omega t)^{\alpha_1 + \alpha_2 + \dots + \alpha_m}}{(m-1 + \alpha_2 + \dots + \alpha_m)! \alpha_1!} p_1^{\alpha_1} b_2^{\alpha_2} \dots b_m^{\alpha_m}. \quad (48)$$

In contrast, differentiation of the power series (35) summand by summand yields the left-hand side

$$\dot{\xi}_{\mathbf{p}}(t) = \sum_{\alpha \in \mathbb{N}^m} \frac{t^{m-1} (i\omega t)^{|\alpha|}}{(m-1 + |\alpha|)!} p_1^{\alpha_1} (p_1 + b_2)^{\alpha_2} \dots (p_1 + b_m)^{\alpha_m}. \quad (49)$$

The crucial difference between these two expressions is that the first integer index  $p_1$  occurs in every factor in (49), while it only occurs isolated in (48). In addition,  $\alpha_1$  is part of the large factorial in the denominator of (49), but is isolated in (48). To prove equivalence of these two series expressions, we will proceed to pull the index  $p_1$  outside of every binomial in (49) and reorder the summations.

Applying the binomial theorem to every factor in (49) yields

$$\begin{aligned} \dot{\xi}_{\mathbf{p}}(t) &= \sum_{\alpha \in \mathbb{N}^m} \frac{t^{m-1} (i\omega t)^{|\alpha|}}{(m-1 + |\alpha|)!} p_1^{\alpha_1} \left( \sum_{n_2=0}^{\alpha_2} \binom{\alpha_2}{n_2} p_1^{\alpha_2 - n_2} b_2^{n_2} \right) \dots \left( \sum_{n_m=0}^{\alpha_m} \binom{\alpha_m}{n_m} p_1^{\alpha_m - n_m} b_m^{n_m} \right) \\ &= \sum_{\alpha \in \mathbb{N}^m} \sum_{n_2=0}^{\alpha_2} \dots \sum_{n_m=0}^{\alpha_m} \frac{t^{m-1} (i\omega t)^{|\alpha|}}{(m-1 + |\alpha|)!} p_1^{(|\alpha| - \sum_{k=2}^m n_k)} b_2^{n_2} \dots b_m^{n_m} \binom{\alpha_2}{n_2} \dots \binom{\alpha_m}{n_m}. \end{aligned} \quad (50)$$

Using  $\sum_{\alpha_k=0}^{\infty} \sum_{n_k=0}^{\alpha_k} = \sum_{n_k=0}^{\infty} \sum_{\alpha_k=n_k}^{\infty}$  for  $k = 2, \dots, m$ , every corresponding pair of sums can be swapped. We introduce the new summation multi-index  $\mathbf{n} = [n_2, \dots, n_m]$ , which starts with  $n_2$ . Correspondingly, the

shifted index  $\tilde{\boldsymbol{\alpha}} = [\tilde{\alpha}_2, \dots, \tilde{\alpha}_m] \in \mathbb{N}^{m-1}$  with  $\tilde{\alpha}_k = \alpha_k - n_k$  also begins with  $\tilde{\alpha}_2$ . Substituted into the series after the sums are swapped, this yields

$$\begin{aligned} \dot{\xi}_{\mathbf{p}}(t) &= \sum_{\mathbf{n} \in \mathbb{N}^{m-1}} \sum_{\alpha_2=n_2}^{\infty} \cdots \sum_{\alpha_m=n_m}^{\infty} \sum_{\alpha_1=0}^{\infty} \frac{t^{m-1}(i\omega t)^{|\boldsymbol{\alpha}|}}{(m-1+|\boldsymbol{\alpha}|)!} p_1^{(|\boldsymbol{\alpha}|-\sum_{k=2}^m n_k)} b_2^{n_2} \cdots b_m^{n_m} \binom{\alpha_2}{n_2} \cdots \binom{\alpha_m}{n_m} \\ &= \sum_{\mathbf{n} \in \mathbb{N}^{m-1}} \sum_{\tilde{\boldsymbol{\alpha}} \in \mathbb{N}^{m-1}} \sum_{\alpha_1=0}^{\infty} \frac{t^{m-1}(i\omega t)^{\alpha_1+|\tilde{\boldsymbol{\alpha}}|+|\mathbf{n}|}}{(m-1+\alpha_1+|\tilde{\boldsymbol{\alpha}}|+|\mathbf{n}|)!} p_1^{\alpha_1+|\tilde{\boldsymbol{\alpha}}|} b_2^{n_2} \cdots b_m^{n_m} \binom{\tilde{\alpha}_2+n_2}{n_2} \cdots \binom{\tilde{\alpha}_m+n_m}{n_m}. \end{aligned} \quad (51)$$

Next, the summation variable  $\alpha_1$  is replaced by  $M = \alpha_1 + |\tilde{\boldsymbol{\alpha}}|$  to yield

$$\dot{\xi}_{\mathbf{p}}(t) = \sum_{\mathbf{n} \in \mathbb{N}^{m-1}} \sum_{\tilde{\boldsymbol{\alpha}} \in \mathbb{N}^{m-1}} \sum_{M=|\tilde{\boldsymbol{\alpha}}|}^{\infty} \frac{t^{m-1}(i\omega t)^{M+|\mathbf{n}|}}{(m-1+M+|\mathbf{n}|)!} p_1^M b_2^{n_2} \cdots b_m^{n_m} \binom{\tilde{\alpha}_2+n_2}{n_2} \cdots \binom{\tilde{\alpha}_m+n_m}{n_m}. \quad (52)$$

Note that only the binomial coefficients and the lower bound of  $M$  depend on the multi-index  $\tilde{\boldsymbol{\alpha}}$ . In the next step, we intend to swap the summation over  $M$  with the summation over  $\tilde{\boldsymbol{\alpha}}$ . For the sake of brevity, we temporarily collect all  $\tilde{\boldsymbol{\alpha}}$ -independent terms of the summand into

$$h(t, M, \mathbf{n}, \mathbf{p}) := \frac{t^{m-1}(i\omega t)^{M+|\mathbf{n}|}}{(m-1+M+|\mathbf{n}|)!} p_1^M b_2^{n_2} \cdots b_m^{n_m}. \quad (53)$$

For all summands it holds that  $M \geq |\tilde{\boldsymbol{\alpha}}|$ . Hence, the value of  $M$  acts as an upper bound on  $|\tilde{\boldsymbol{\alpha}}|$ . In other words, for any fixed value  $M$ ,  $\tilde{\alpha}_2$  can take any value that is not larger than  $M$ . Then, for fixed  $M$  and  $\tilde{\alpha}_2$ , the value of  $\tilde{\alpha}_3$  can be at most  $M - \tilde{\alpha}_2$ , and this procedure can be continued to pull the summation over  $M$  to the front and yield

$$\dot{\xi}_{\mathbf{p}}(t) = \sum_{\mathbf{n} \in \mathbb{N}^{m-1}} \sum_{M=0}^{\infty} h(t, M, \mathbf{n}, \mathbf{p}) \sum_{\tilde{\alpha}_2=0}^M \sum_{\tilde{\alpha}_3=0}^{M-\tilde{\alpha}_2} \cdots \sum_{\tilde{\alpha}_m=0}^{M-\tilde{\alpha}_2-\cdots-\tilde{\alpha}_{m-1}} \binom{\tilde{\alpha}_2+n_2}{n_2} \cdots \binom{\tilde{\alpha}_m+n_m}{n_m}. \quad (54)$$

The  $m-1$  right-most summations are covered by Lemma 12 of Appendix A, so all summation indices  $\tilde{\alpha}_k$  for  $k=2, \dots, m$  can be eliminated:

$$\dot{\xi}_{\mathbf{p}}(t) = \sum_{\mathbf{n} \in \mathbb{N}^{m-1}} \sum_{M=0}^{\infty} h(t, M, \mathbf{n}, \mathbf{p}) \binom{M+(m-1)+|\mathbf{n}|}{M}. \quad (55)$$

Re-substituting  $h(t, M, \mathbf{n}, \mathbf{p})$  and writing the binomial coefficient in factorial form yields

$$\begin{aligned} \dot{\xi}_{\mathbf{p}}(t) &= \sum_{\mathbf{n} \in \mathbb{N}^{m-1}} \sum_{M=0}^{\infty} \frac{t^{m-1}(i\omega t)^{M+|\mathbf{n}|}}{(m-1+M+|\mathbf{n}|)!} p_1^M b_2^{n_2} \cdots b_m^{n_m} \frac{(M+(m-1)+|\mathbf{n}|)!}{M!(m-1+|\mathbf{n}|)!} \\ &= \sum_{\mathbf{n} \in \mathbb{N}^{m-1}} \sum_{M=0}^{\infty} \frac{t^{m-1}(i\omega t)^{M+|\mathbf{n}|}}{(m-1+|\mathbf{n}|)! M!} p_1^M b_2^{n_2} \cdots b_m^{n_m}. \end{aligned} \quad (56)$$

Comparison of (56) to (48) reveals  $\dot{\xi}_{\mathbf{p}}(t) = \xi_{[p_2, \dots, p_m]}(t) e^{ip_1 \omega t}$ , concluding Case 2.  $\square$

Appendix C examines a consequence of Lemma 3, namely that  $\xi_{\mathbf{p}}$  is  $T$ -periodic with finite support of Fourier coefficients for most values of  $\mathbf{p}$ . This periodicity property is, however, not of immediate use for the further developments and is therefore deferred to the appendix. In the next subsection, we use Lemma 3 directly as a tool to show that the series representation (34) fulfills the differential equation (2).

#### 4.2. Proof of Theorem 1

After having examined the scalar factor, we are now ready to prove Theorem 1.

*Proof.* We begin by showing that the series (34) is absolutely convergent. In a second step we will show that this series solves the matrix differential equation (2), guaranteeing that it is indeed the fundamental matrix. By Lemma 2 and Assumption 1, the norm of a summand of (34) is bounded by

$$\|\xi_{\mathbf{p}}(t) \mathcal{J}_{\mathbf{p}}\| \leq \|\xi_{\mathbf{p}}(t)\| \|\mathcal{J}_{\mathbf{p}}\| \leq \frac{|t|^m}{m!} a^m e^{-b|\mathbf{p}|} = \frac{|at|^m}{m!} e^{-b|\mathbf{p}|}. \quad (57)$$

Analogously as in the proof for Lemma 2, this bound only involves the norm of the integer index tuple  $\mathbf{p}$ . Hence, the sum over all integer index tuples  $\mathbf{p}$  can be reduced to the sum over their norm  $M = |\mathbf{p}|$ , using Lemma 10ii) of Appendix A to count the number of tuples with a given norm  $M$ . This yields

$$\sum_{\mathbf{p} \in \mathbb{Z}^m} \|\xi_{\mathbf{p}}(t) \mathcal{J}_{\mathbf{p}}\| \leq \sum_{M=0}^{\infty} \sum_{\substack{\mathbf{p} \in \mathbb{Z}^m \\ |\mathbf{p}|=M}} \frac{|at|^m}{m!} e^{-bM} \leq \sum_{M=0}^{\infty} \frac{|2at|^m}{m!} \binom{M+m-1}{m-1} e^{-bM}. \quad (58)$$

After pulling out the factor  $\frac{|2at|^m}{m!}$ , the series on the right-hand side is of the form  $\sum_{M=0}^{\infty} \binom{M+k}{k} M^q x^M$  with  $q = 0$ ,  $k = m - 1$  and  $x = e^{-b} < 1$ . This is the Taylor series of  $(1-x)^{-(1+k)}$ , treated in Lemma 13 of Appendix B. Hence, the closed-form solution is

$$\sum_{\mathbf{p} \in \mathbb{Z}^m} \|\xi_{\mathbf{p}}(t) \mathcal{J}_{\mathbf{p}}\| \leq \frac{|2at|^m}{m!} \sum_{M=0}^{\infty} \binom{M+m-1}{m-1} e^{-bM} = \frac{|2at|^m}{m!} (1 - e^{-b})^{-m}. \quad (59)$$

Absolute convergence follows by

$$1 + \sum_{m=1}^{\infty} \sum_{\mathbf{p} \in \mathbb{Z}^m} \|\xi_{\mathbf{p}}(t) \mathcal{J}_{\mathbf{p}}\| \leq 1 + \sum_{m=1}^{\infty} \frac{1}{m!} \left( \frac{|2at|}{1 - e^{-b}} \right)^m = \exp \left( \frac{|2at|}{1 - e^{-b}} \right). \quad (60)$$

We are now ready to show that (34) satisfies the matrix differential equation (2). As  $\xi_{\mathbf{p}}(0) = 0$  for arbitrary  $m \in \mathbb{N} \setminus \{0\}$  and  $\mathbf{p} \in \mathbb{Z}^m$ , the initial condition  $\Phi(0) = \mathbf{I}$  is trivially satisfied. Differentiation of the series summand by summand yields the derivative

$$\dot{\Phi}(t) = \sum_{m=1}^{\infty} \sum_{\mathbf{p} \in \mathbb{Z}^m} \dot{\xi}_{\mathbf{p}}(t) \mathcal{J}_{\mathbf{p}}, \quad (61)$$

and the right-hand side of the matrix differential equation (2) reads

$$\begin{aligned} \mathbf{J}(t) \Phi(t) &= \left( \sum_{k=-\infty}^{\infty} \mathbf{J}_k e^{ik\omega t} \right) \left( \mathbf{I} + \sum_{m=1}^{\infty} \sum_{\mathbf{p} \in \mathbb{Z}^m} \xi_{\mathbf{p}}(t) \mathcal{J}_{\mathbf{p}} \right) \\ &= \sum_{p=-\infty}^{\infty} e^{ip\omega t} \mathbf{J}_p + \sum_{m=1}^{\infty} \sum_{k=-\infty}^{\infty} \sum_{\mathbf{p} \in \mathbb{Z}^m} \xi_{\mathbf{p}}(t) e^{ik\omega t} \mathbf{J}_k \mathcal{J}_{\mathbf{p}}. \end{aligned} \quad (62)$$

With new integer index tuples  $\tilde{\mathbf{p}} := [k, \mathbf{p}] \in \mathbb{Z}^{m+1}$  and an index shift from  $m+1$  to  $m$ , this expression can be reformulated to

$$\mathbf{J}(t) \Phi(t) = \sum_{p=-\infty}^{\infty} e^{ip\omega t} \mathbf{J}_p + \sum_{m=2}^{\infty} \sum_{\tilde{\mathbf{p}} \in \mathbb{Z}^m} \xi_{[\tilde{p}_2, \dots, \tilde{p}_m]}(t) e^{i\tilde{p}_1 \omega t} \mathcal{J}_{\tilde{\mathbf{p}}}. \quad (63)$$

Comparison of (61) and (63) reveals that the matrix differential equation (1) is satisfied if the following conditions on  $\xi$  hold:

- 1)  $\dot{\xi}_p(t) = e^{ip\omega t}$  if  $p \in \mathbb{Z}$
- 2)  $\dot{\xi}_{\mathbf{p}}(t) = \xi_{[p_2, \dots, p_m]} e^{ip_1 \omega t}$  if  $\mathbf{p} \in \mathbb{Z}^m$  with  $m \geq 2$ .

As these conditions are true due to Lemma 3, the series (34) does indeed solve the matrix differential equation (1). This linear differential equation only has one unique solution, which must thus be the fundamental solution matrix.  $\square$

#### 4.3. Series expression for Koopman-Hill approximation

The main benefit of the series expression (34) is that we can bring the Koopman-Hill approximation into the same format and then compare both series term-by-term. To enable similar arguments as in Section 4.2, we will first derive a linear matrix differential equation that is satisfied by the Koopman-Hill projection.

The Koopman-Hill approximation (17a) of the fundamental solution matrix  $\Phi(t)$  is the centermost block of the tall matrix  $e^{\mathbf{H}t}\mathbf{W}$ . Due to (11), any other  $j$ -th block of  $e^{\mathbf{H}t}\mathbf{W}$ ,  $j = -N, \dots, N$ , approximates  $\Phi(t)e^{-ij\omega t}$ . In words, the blocks of  $e^{\mathbf{H}t}\mathbf{W}$  approximate the fundamental solution matrix, divided by the corresponding Fourier term. These Fourier terms can be offset by the matrix  $\mathbf{D} = \text{diag}\{-N, \dots, N\} \otimes \mathbf{I}$ , such that the matrix

$$\mathbf{Q}(t) := e^{i\omega\mathbf{D}t}e^{\mathbf{H}t}\mathbf{W} \quad (64)$$

is of the same size as  $\mathbf{W}$  and every block  $\mathbf{Q}_j$ ,  $j = -N, \dots, N$ , offers an approximation of the fundamental solution matrix. While all these blocks approximate the same quantity  $\Phi(t)$ , their individual values and their individual approximation errors may differ. We will call  $\mathbf{Q}_j$  the  $j$ -shifted approximation of  $\Phi(t)$ . Correspondingly, the direct Koopman-Hill projection (17a) is the 0-shifted approximation. Differentiating (64) reveals the linear matrix initial value problem

$$\dot{\mathbf{Q}}(t) = (i\omega\mathbf{D} + e^{i\omega\mathbf{D}t}\mathbf{H}e^{-i\omega\mathbf{D}t})\mathbf{Q}(t) \quad \mathbf{Q}(0) = \mathbf{W}, \quad (65)$$

whose unique solution is  $\mathbf{Q}(t)$ .

The following theorem provides a general series expression for the  $j$ -shifted Koopman-Hill approximation.

**Theorem 4** (Series expression for the shifted Koopman-Hill approximations). *For any index  $j \in \{-N, \dots, N\}$ , the  $j$ -th block of the matrix  $\mathbf{Q}(t) = e^{i\omega\mathbf{D}t}e^{\mathbf{H}t}\mathbf{W}$  collecting all the shifted Koopman-Hill approximations is given by the series*

$$\mathbf{Q}_j(t) = \mathbf{I} + \sum_{m=1}^{\infty} \sum_{\mathbf{p} \in \mathcal{P}_j^{(m)}} \xi_{\mathbf{p}}(t)\mathcal{J}_{\mathbf{p}}, \quad (66)$$

where

$$\mathcal{P}_j^{(m)} = \left\{ \mathbf{p} \in \mathbb{Z}^m : \left| j - \sum_{l=1}^m p_l \right| \leq N \text{ for all } w = 1, \dots, m \right\} \quad (67)$$

is the set of admissible integer index tuples and  $\xi_{\mathbf{p}}(t)$  is the scalar factor defined in Theorem 1. The series (66) is absolutely convergent for all  $t \in \mathbb{R}$  if all Fourier coefficients  $\{\mathbf{J}_k\}_{k=-2N, \dots, 2N}$  that occur in  $\mathbf{H}$  are bounded.

Geometrically, the sets  $\mathcal{P}_j^{(m)}$  appear as parallelotopes, i.e.,  $m$ -dimensional parallelograms, centered around the point  $(j, 0, \dots, 0)$ . This explains the terminology of *shifted* Koopman-Hill approximations. Figure 3 visualizes the parallelograms for the case  $m = 2$ .

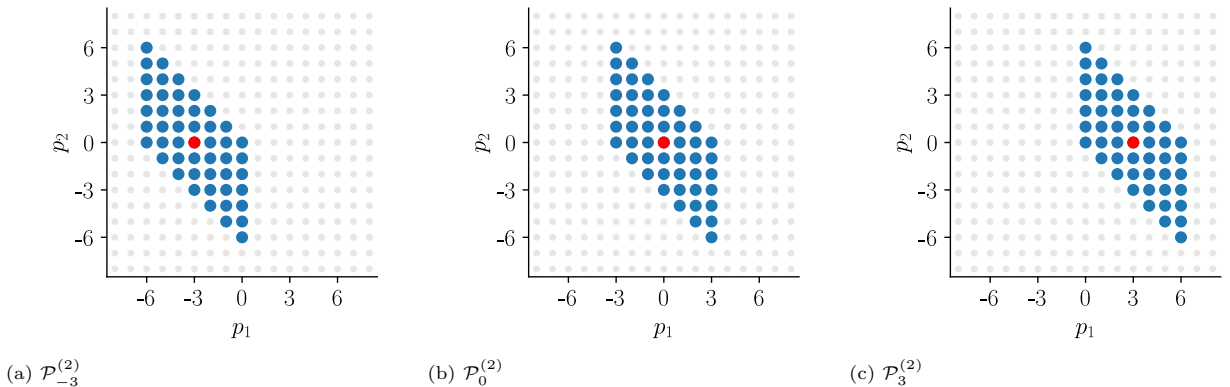


Figure 3: Visualization of the sets  $\mathcal{P}_j^{(2)}$  with  $N = 3$  for different values of  $j$ . Center element located at  $(j, 0)$  is indicated by a red dot.

The figure suggests that all sets  $\mathcal{P}_j^{(m)}$  are subsets of the  $m$ -hypercube centered at zero with edge length  $4N$ , i.e., any entry  $p_k$  of an applicable multi-index must fulfill  $|p_k| \leq 2N$ . This is indeed the case: Applying the inverse triangle inequality to the sum  $\sum_{l=1}^k p_l$  for an entry  $p_k$  with  $|p_k| = M > 2N$  yields

$$\left| j - \sum_{l=1}^k p_l \right| \geq \left| \left| j - \sum_{l=1}^{k-1} p_l \right| - |p_k| \right| \geq |N - M| > N, \quad (68)$$

which contradicts the condition of  $\mathcal{P}_j^{(m)}$ . This is expected as Fourier coefficients  $\mathbf{J}_p$  with  $p > 2N$  do not appear in the Hill matrix and can therefore not influence  $e^{\mathbf{H}t}\mathbf{W}$ .

*Proof.* The series (66) converges absolutely as

$$\sum_{m=1}^{\infty} \sum_{\mathbf{p} \in \mathcal{P}_j^{(m)}} \|\xi_{\mathbf{p}}(t)\mathcal{J}_{\mathbf{p}}\| \leq \sum_{m=1}^{\infty} \sum_{\mathbf{p} \in \mathbb{Z}^m} \|\xi_{\mathbf{p}}(t)\mathcal{J}_{\mathbf{p}}\|, \quad (69)$$

where the right-hand side converges absolutely due to Theorem 1.

It remains to show that the right-hand side of (66) fulfills the matrix initial value problem (65). The initial condition is trivially satisfied. For the differential equation, the approach is analogous to the proof for Theorem 1, only the summation limits have to be considered carefully now.

The  $jk$ -th block of the time-periodic matrix  $(i\omega\mathbf{D} + e^{i\omega\mathbf{D}t}\mathbf{H}e^{-i\omega\mathbf{D}t})$  is

$$(i\omega\mathbf{D} + e^{i\omega\mathbf{D}t}\mathbf{H}e^{-i\omega\mathbf{D}t})_{jk} = \mathbf{J}_{j-k}e^{i(j-k)\omega t} \quad (70)$$

as the matrix  $i\omega\mathbf{D}$  removes the  $i\omega$ -terms in  $\mathbf{H}$  and pre-multiplication with the diagonal matrix  $e^{i\omega\mathbf{D}t}$  scales the rows of  $\mathbf{H}$ , while post-multiplication with  $e^{-i\omega\mathbf{D}t}$  scales the columns. For the purpose of this proof, we will call the right-hand side of (65)  $\hat{\mathbf{Q}}$  if the series expression for  $\mathbf{Q}$  is used, as we do not (yet) know that it actually coincides with  $\mathbf{Q}$ . Evaluating the matrix multiplication block by block yields

$$\hat{\mathbf{Q}}_j(t) := [(i\omega\mathbf{D} + e^{i\omega\mathbf{D}t}\mathbf{H}e^{-i\omega\mathbf{D}t})\mathbf{Q}(t)]_j = \sum_{l=-N}^N \mathbf{J}_{j-l}e^{i(j-l)\omega t} \left( \mathbf{I} + \sum_{m=1}^{\infty} \sum_{\mathbf{p} \in \mathcal{P}_l^{(m)}} \xi_{\mathbf{p}}(t)\mathcal{J}_{\mathbf{p}} \right) \quad (71)$$

or, after the index shift  $\tilde{p}_1 = j - l$  and some reorganization,

$$\hat{\mathbf{Q}}_j(t) = \sum_{\tilde{p}_1=j-N}^{j+N} \mathbf{J}_{\tilde{p}_1}e^{i\tilde{p}_1\omega t} + \sum_{m=1}^{\infty} \sum_{\tilde{p}_1=j-N}^{j+N} \sum_{[p_1, \dots, p_m] \in \mathcal{P}_{j-\tilde{p}_1}^{(m)}} \xi_{[p_1, \dots, p_m]}(t) e^{i\tilde{p}_1\omega t} \mathbf{J}_{\tilde{p}_1} \mathcal{J}_{\mathbf{p}}. \quad (72)$$

With the relabeling  $[p_1, \dots, p_m] := [\tilde{p}_2, \dots, \tilde{p}_{m+1}]$  and the index shift in  $m$  by one, the expression

$$\hat{\mathbf{Q}}_j(t) = \sum_{\tilde{p}_1=j-N}^{j+N} \mathbf{J}_{\tilde{p}_1}e^{i\tilde{p}_1\omega t} + \sum_{m=2}^{\infty} \sum_{\tilde{p}_1=j-N}^{j+N} \sum_{[\tilde{p}_2, \dots, \tilde{p}_m] \in \mathcal{P}_{j-\tilde{p}_1}^{(m-1)}} \xi_{[\tilde{p}_2, \dots, \tilde{p}_m]}(t) e^{i\tilde{p}_1\omega t} \mathbf{J}_{\tilde{p}_1} \mathcal{J}_{[\tilde{p}_2, \dots, \tilde{p}_m]} \quad (73)$$

$$= \sum_{p=j-N}^{j+N} \mathbf{J}_p \dot{\xi}_p(t) + \sum_{m=2}^{\infty} \sum_{\tilde{p}_1=j-N}^{j+N} \sum_{[\tilde{p}_2, \dots, \tilde{p}_m] \in \mathcal{P}_{j-\tilde{p}_1}^{(m-1)}} \dot{\xi}_{\tilde{\mathbf{p}}}(t) \mathcal{J}_{\tilde{\mathbf{p}}} \quad (74)$$

follows, where the derivative properties of Lemma 3 were used in the second step. This series is analogous to (63) in Theorem 1, but with nontrivial limits in the sum. Evaluating the left-hand side of (65) by differentiating (66) yields

$$\dot{\mathbf{Q}}_j(t) = \sum_{m=1}^{\infty} \sum_{\mathbf{p} \in \mathcal{P}_j^{(m)}} \dot{\xi}_{\mathbf{p}}(t) \mathcal{J}_{\mathbf{p}}, \quad (75)$$

which is in turn analogous to (61). The comparison of (74) and (75) reveals that the two expressions coincide if the summation sets  $\mathcal{P}_j^{(m)}$  and  $\left\{ \mathbf{p} : |j - p_1| \leq N, [p_2, \dots, p_m] \in \mathcal{P}_{j-p_1}^{(m-1)} \right\}$  are equal. With

$$\mathbf{p} \in \mathcal{P}_j^{(m)} \iff |j - p_1| \leq N \text{ and } \left| j - p_1 - \sum_{k=1}^w p_{k+1} \right| \leq N \text{ for all } w = 1, \dots, m-1 \quad (76)$$

$$\iff p_1 \in \{j - N, \dots, j + N\} \text{ and } [p_2, \dots, p_m] \in \mathcal{P}_{j-p_1}^{(m-1)}, \quad (77)$$

this is indeed the case and the series (66) solves the matrix differential equation (65).  $\square$

The series expression for the direct Koopman-Hill projection follows immediately from Theorem 4 for  $j = 0$ .

**Corollary 5** (Direct Koopman-Hill projection). *The direct Koopman-Hill projection approximation as introduced in (17a),  $\mathbf{C}e^{\mathbf{H}t}\mathbf{W} = \mathbf{Q}_0(t)$ , is given by the series*

$$\mathbf{C}e^{\mathbf{H}t}\mathbf{W} = \mathbf{I} + \sum_{m=1}^{\infty} \sum_{\mathbf{p} \in \mathcal{P}_0^{(m)}} \xi_{\mathbf{p}}(t) \mathcal{J}_{\mathbf{p}} \quad (78)$$

with the index parallelotopes

$$\mathcal{P}_0^{(m)} = \left\{ \mathbf{p} \in \mathbb{Z}^m : \left| \sum_{l=1}^w p_l \right| \leq N \text{ for all } w = 1, \dots, m \right\}. \quad (79)$$

## 5. Error bound and convergence guarantee

The previous section derived the series formulations (34) and (78) for the true fundamental solution matrix and the direct Koopman-Hill projection, respectively. Notably, both series are characterized by the same monomials  $\mathcal{J}_{\mathbf{p}}$  and identical scalar factors  $\xi_{\mathbf{p}}(t)$ . The only difference is that the Koopman-Hill approximation (78) is a partial sum of the true fundamental solution matrix (34) due to the truncation effects. Consequently, the truncation error  $\mathbf{E}(t)$  can be expressed as the series over all multi-indices that are *not* included in the series (78), i.e.,

$$\mathbf{E}(t) = \Phi(t) - \mathbf{C}e^{\mathbf{H}t}\mathbf{W} = \sum_{m=1}^{\infty} \sum_{\mathbf{p} \in \mathbb{Z}^m \setminus \mathcal{P}_0^{(m)}} \xi_{\mathbf{p}}(t) \mathcal{J}_{\mathbf{p}}. \quad (80)$$

This section is dedicated to our main result, bounding (80) to provide a convergence guarantee for the Koopman-Hill approximation.

**Theorem 6** (Error bound and convergence of the direct Koopman-Hill projection approximation). *Let Assumption 1 hold. For  $b > \ln 2$  and for a fixed truncation order  $N \in \mathbb{N}$ , the approximation error between the true fundamental solution matrix and the direct Koopman-Hill projection (17a) is bounded by*

$$\|\Phi(t) - \mathbf{C}e^{\mathbf{H}t}\mathbf{W}\| \leq (2e^{-b})^N e^{|4at|}. \quad (81)$$

*This error bound decays exponentially with  $N$ , providing a convergence guarantee of the Koopman-Hill projection. Satisfaction of a desired accuracy  $\|\Phi(t) - \mathbf{C}e^{\mathbf{H}t}\mathbf{W}\| \leq E_{\text{des}}$  is guaranteed if the truncation order fulfills*

$$N \geq N^* = \frac{|4at| - \ln(E_{\text{des}})}{b - \ln 2}. \quad (82)$$

*Remark.* The condition  $b > \ln 2$  for the applicability of the closed-form bound (81) is more conservative than the conditions needed for convergence of the series for  $\Phi(t)$  and  $\mathbf{C}e^{\mathbf{H}t}\mathbf{W}$ . In practice, satisfaction of this condition can be determined numerically. This will be illustrated in Section 7 with the help of two numerical examples.

*Proof.* In a first step, we bound each summand of the approximation error (80) individually using (57) and Assumption 1 to obtain

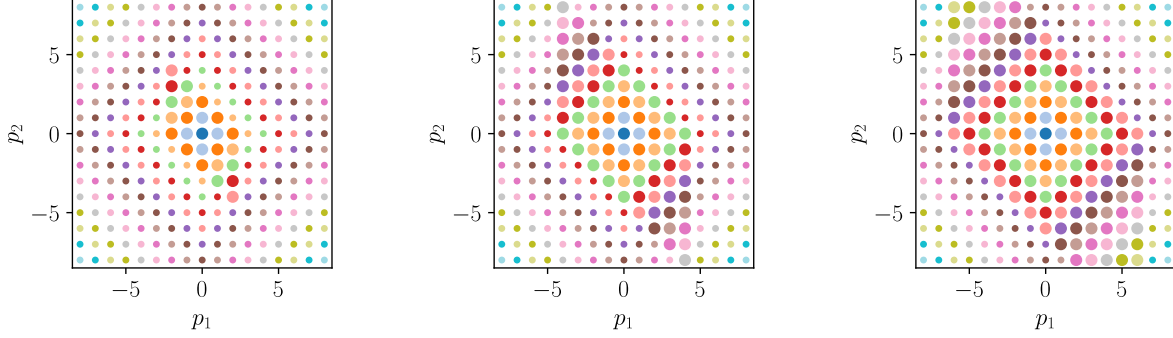
$$\|\mathbf{E}(t)\| \leq \sum_{m=1}^{\infty} \sum_{\mathbf{p} \in \mathbb{Z}^m \setminus \mathcal{P}_0^{(m)}} \|\xi_{\mathbf{p}}(t) \mathcal{J}_{\mathbf{p}}\| \leq \sum_{m=1}^{\infty} \sum_{\mathbf{p} \in \mathbb{Z}^m \setminus \mathcal{P}_0^{(m)}} \frac{|at|^m}{m!} e^{-b|\mathbf{p}|}. \quad (83)$$

As in the proof of Theorem 1, only the norm  $|\mathbf{p}|$  of each integer index tuple appears in the summand, allowing to replace the sum over all integer index tuples by a sum over their norm. This reformulation yields the triple sum

$$\|\mathbf{E}(t)\| \leq \sum_{m=1}^{\infty} \frac{|at|^m}{m!} \sum_{M=0}^{\infty} e^{-bM} \sum_{\substack{\mathbf{p} \in \mathbb{Z}^m \setminus \mathcal{P}_0^{(m)} \\ |\mathbf{p}|=M}} 1, \quad (84)$$



where the rightmost sum represents the number of integer index tuples that lie outside  $\mathcal{P}_0^{(m)}$ . In Figure 4, these tuples are visualized for  $m = 2$  and and three different values of  $N$ . Dots of equal color have equal norm  $|\mathbf{p}|$  and large dots are represented in  $\mathcal{P}_0^{(2)}$ , while small dots are not. Therefore, the number of integer index tuples counted in (84) is the number of small dots of a given color in Figure 4. There is no closed-form expression for this number. However, the figure shows that for all  $M \leq N$ , the whole rhombus corresponding to norm  $M$  is contained inside the set  $\mathcal{P}_0^{(2)}$ . Hence, these values of  $M$  do not contribute to the sum (84) at all.



(a)  $N = 2$ : Orange rhombus ( $|\mathbf{p}| = 2$ )  $\subset \mathcal{P}_0^{(2)}$ . (b)  $N = 4$ : Green rhombus ( $|\mathbf{p}| = 4$ )  $\subset \mathcal{P}_0^{(2)}$ . (c)  $N = 6$ : Pink rhombus ( $|\mathbf{p}| = 6$ )  $\subset \mathcal{P}_0^{(2)}$ .

Figure 4: Visualization of integer index set and 1-norm. Dots of equal color have equal 1-norm. Large dots are elements of  $\mathcal{P}_0^{(2)}$  with the chosen truncation order  $N$ , while small dots are not.

This observation can be generalized to all  $m \in \mathbb{N} \setminus \{0\}$ . Any index tuple  $\mathbf{p} \in \mathbb{Z}^m$  that has a norm  $|\mathbf{p}| = \sum_{k=1}^m |p_k| = M \leq N$  is automatically contained in  $\mathcal{P}_0^{(m)}$  by its definition (79). Consequently, the middle series in (84) may be initialized at  $M = N + 1$  instead of  $M = 0$  without losing any summands. For the remaining values of  $M$ , we upperbound the sum by simply counting *all* possible integer index tuples with norm  $M$  instead of just those which are not contained in  $\mathcal{P}_0^{(m)}$ . Then Lemma 10ii) can be used to bound the number of such tuples. The series (84) can thus be upperbounded by

$$\|\mathbf{E}(t)\| \leq \sum_{m=1}^{\infty} \frac{|at|^m}{m!} \sum_{M=N+1}^{\infty} \sum_{\substack{\mathbf{p} \in \mathbb{Z}^m \\ |\mathbf{p}|=M}} e^{-bM} \leq \sum_{m=1}^{\infty} \frac{|2at|^m}{m!} \sum_{M=N+1}^{\infty} \binom{M+m-1}{m-1} e^{-bM}. \quad (85)$$

The rightmost series in (85) is the remainder  $R_N(x)$  of the Taylor series of  $(1-x)^{-(k+1)}$ , treated in Lemma 13 of Appendix B, with  $x = e^{-b} < 1$  and  $k = m - 1$ . Using the expression (B.3) for the remainder and keeping  $x$  for the sake of brevity, we obtain

$$\|\mathbf{E}(t)\| \leq x^N \sum_{m=1}^{\infty} \frac{|2at|^m}{m!} \sum_{w=1}^m \binom{N+m}{N+w} \left(\frac{x}{1-x}\right)^w. \quad (86)$$

The assumption  $b > \ln 2$  guarantees that  $x < 0.5$ , and thus  $\frac{x}{1-x} < 1$ . Summing the binomial coefficients from 0 to  $N + m$  instead of from  $N + 1$  to  $N + m$  yields the bound

$$\begin{aligned} \|\mathbf{E}(t)\| &\leq x^N \sum_{m=1}^{\infty} \frac{|2at|^m}{m!} \sum_{w=0}^{m+N} \binom{m+N}{w} \\ &= x^N \sum_{m=1}^{\infty} \frac{|2at|^m}{m!} 2^{m+N} \\ &= (2x)^N e^{4a|t|} \\ &= (2e^{-b})^N e^{4at}. \end{aligned} \quad (87)$$

This is the desired error bound (81). The expression (82) for the minimum truncation order  $N^*$  which guarantees an error smaller than  $E_{\text{des}}$  follows immediately by isolating  $N^*$  in  $E_{\text{des}} = (2e^{-b})^{N^*} e^{4at}$ .  $\square$

Before discussing the implications of this error bound, we will introduce and discuss a modified, subharmonic formulation in the following section.

## 6. Subharmonics for improved convergence rate

In the Koopman-Hill framework, a projection is needed to go back from the lifted variables  $\mathbf{z}$  to the original variables  $\mathbf{y}$ . In the previous sections, the most straightforward of these projections was chosen: Simply considering the centermost block of entries,  $\mathbf{z}_0$ , whose corresponding observable is immediately given by  $\mathbf{y}(t)$ . However, as the other blocks of observables are of the form  $\mathbf{z}_k \approx \mathbf{y}(t)e^{-ik\omega t}$ , other projections of the form  $\mathbf{y} \approx \sum_{k=-N}^N c_k e^{ik\omega t} \mathbf{z}_k$  could also be constructed, as long as the normalization condition  $\sum_{k=-N}^N c_k = 1$  is fulfilled. Such nontrivial projections are considered in this section. Specifically, in Section 6.1, we demonstrate that the direct projection is best for general  $\mathbf{J}(t)$ .

Previous works of the authors [13, 14] have observed that in the case where every odd Fourier coefficient is zero it is indeed more beneficial numerically to use a nontrivial projection. We will formalize this approach, which we call the *subharmonic* approach, in Section 6.2 and show in Section 6.3 that this is not only beneficial numerically, but also comes with a lower error bound compared to the direct approach.

### 6.1. Other non-subharmonic projections

As discussed in Section 4.3, all blocks of  $\mathbf{Q}(t) = e^{i\omega \mathbf{D}t} e^{\mathbf{H}t} \mathbf{W}$  approximate the true fundamental solution matrix. Correspondingly, any normalized linear combination between them can be used as an approximation.

In Figure 3 of Section 4.3 it became clear that all such blocks  $\mathbf{Q}_j$  have as their index sets parallelotopes, but with a shifted center point. Repeating the argumentation from Section 5 reveals that the rhombus of considered integer indices is largest for the most centered parallelotope. In addition, choosing as approximation just one block of  $\mathbf{Q}$  ensures that all summands of (34) are either met perfectly or not at all. This is not the case for any other linear combination of the blocks, where some summands would only be met partially. Hence, for general applications, the direct projection is best.

### 6.2. Formulation of the subharmonic projection

The discussions in the previous sections assumed that all monomials  $\mathcal{J}_{\mathbf{p}}$  may be nonzero. If every odd Fourier coefficient vanishes, the optimal projection changes. On first glance, this may seem like a very special class of problems. However, for an arbitrary  $T$ -periodic  $\mathbf{J}(t)$ , this property can be enforced by noting that  $\mathbf{J}(t)$  is necessarily also periodic with period  $\tilde{T} := 2T$ . This *subharmonic* period and its corresponding subharmonic Fourier series can also be used to construct a Hill matrix. In this section, all subharmonic quantities constructed using this argument are indicated by a tilde to differentiate them from the quantities without the tilde, which are related to the original period time.

The subharmonic period  $\tilde{T} = 2T$  has a corresponding base frequency  $\tilde{\omega} = \frac{2\pi}{2T} = \frac{\omega}{2}$ , which defines the subharmonic Fourier series

$$\mathbf{J}(t) = \sum_{\tilde{k}=-\infty}^{\infty} \tilde{\mathbf{J}}_{\tilde{k}} e^{i\tilde{k}\frac{\omega}{2}t}. \quad (88)$$

Comparison of (88) with the original Fourier series  $\mathbf{J}(t) = \sum_{k \in \mathbb{Z}} \mathbf{J}_k e^{ik\omega t}$  reveals that every odd subharmonic Fourier coefficient vanishes:

$$\tilde{\mathbf{J}}_{\tilde{k}} = \begin{cases} \mathbf{J}_{\frac{\tilde{k}}{2}} & \text{if } \tilde{k} \text{ even} \\ \mathbf{0} & \text{if } \tilde{k} \text{ odd} \end{cases}. \quad (89)$$

The subharmonic Hill matrix  $\tilde{\mathbf{H}}$  of truncation order  $\tilde{N}$  can be constructed from the subharmonic Fourier series (88) in the usual way by placing the subharmonic Fourier coefficients  $\tilde{\mathbf{J}}_{\tilde{k}}$  with  $\tilde{k} \in \{-2\tilde{N}, \dots, 2\tilde{N}\}$  on the corresponding block diagonals and adding purely imaginary terms of the form  $i\tilde{k}\tilde{\omega}$  in the main diagonal, cf. (13).

For an even subharmonic truncation order  $\tilde{N} = 2N$ , the Fourier coefficients  $\tilde{\mathbf{J}}_{-2\tilde{N}}, \dots, \tilde{\mathbf{J}}_{2\tilde{N}}$  that are represented in the subharmonic Hill matrix can be related to the original Fourier coefficients using (89):

$$(\tilde{\mathbf{J}}_{-4N}, \dots, \tilde{\mathbf{J}}_{4N}) = (\mathbf{J}_{-2N}, \mathbf{0}, \mathbf{J}_{-2N+1}, \mathbf{0}, \dots, \mathbf{J}_{2N-1}, \mathbf{0}, \mathbf{J}_{2N}). \quad (90)$$

In other words, alongside the direct Hill matrix  $\mathbf{H}$  with truncation order  $N$  and base frequency  $\omega$  there also exists the subharmonic Hill matrix  $\tilde{\mathbf{H}}$  of truncation order  $\tilde{N} = 2N$  and base frequency  $\tilde{\omega} = \frac{\omega}{2}$ , which is of twice the size and encodes the same frequency information about  $\mathbf{J}(t)$ , but all nontrivial Fourier coefficient



where  $\mathbf{W}$  is a stack of  $2N + 1$  identity matrices as before, and  $\hat{\mathbf{W}}$  is a stack of  $2N$  identity matrices. As two matrix exponentials of almost same size must be evaluated, this procedure is about twice as costly as evaluating the naive projection.

### 6.3. Series expression of the subharmonic projection

In this section, we use the series expressions of Theorem 4 for the  $\mathbf{Q}_j$  to express the subharmonic Koopman-Hill projection (91) as a series. To achieve this, we bring the scalar factors  $\xi_{\mathbf{p}}(t)$  and the integer index sets  $\mathcal{P}_j^{(m)}$  into subharmonic formulation by replacing  $N$  and  $\omega$  by their subharmonic pendants. Expressed in terms of the original quantities, this yields

$$\tilde{\mathcal{P}}_{\tilde{j}}^{(m)} = \left\{ \tilde{\mathbf{p}} \in \mathbb{Z}^m : \left| \tilde{j} - \sum_{i=1}^m \tilde{p}_i \right| \leq 2N \text{ for all } w = 1, \dots, m \right\} \quad \tilde{j} = -2N, \dots, 2N \quad (97)$$

$$\tilde{\xi}_{\tilde{\mathbf{p}}}(t) = \sum_{\boldsymbol{\alpha} \in \mathbb{N}^m} \frac{t^{m+|\boldsymbol{\alpha}|}}{(m+|\boldsymbol{\alpha}|)!} \left( \frac{i\omega}{2} \right)^{|\boldsymbol{\alpha}|} [\tilde{p}_1, \dots, \tilde{p}_m]^{\boldsymbol{\alpha}} \quad \tilde{\mathbf{p}} \in \mathbb{Z}^m. \quad (98)$$

As  $\tilde{\mathbf{J}}_{\tilde{k}}$  vanishes for all odd  $\tilde{k} \in \mathbb{Z}$ , products  $\tilde{\mathcal{J}}_{\tilde{\mathbf{p}}}$  can only be nonzero if all entries of  $\tilde{\mathbf{p}} \in \mathbb{Z}^m$  are even, which is the case if and only if there exists an integer index tuple  $\mathbf{p} \in \mathbb{Z}^m$  with  $\tilde{\mathbf{p}} = 2\mathbf{p}$ . Note that (98) implies  $\tilde{\xi}_{2\mathbf{p}}(t) = \xi_{\mathbf{p}}(t)$ . If only the even entries are considered, the sets  $\tilde{\mathcal{P}}$  also simplify:

$$\begin{aligned} \tilde{\mathcal{P}}_{\tilde{j}, \text{even}}^{(m)} &:= \left\{ \tilde{\mathbf{p}} \in \tilde{\mathcal{P}}_{\tilde{j}}^{(m)} : \tilde{p}_i \text{ even for all } i = 1, \dots, m \right\} \\ &= 2 \left\{ \mathbf{p} \in \mathbb{Z}^m : \left| \frac{\tilde{j}}{2} - \sum_{i=1}^m p_i \right| \leq N \text{ for all } w = 1, \dots, m \right\}. \end{aligned} \quad (99)$$

$$= 2\mathcal{P}_{\frac{\tilde{j}}{2}}^{(m)}. \quad (100)$$

Here, we re-used the definition (79), but now with potentially non-integer values for  $j$ . All these insights allow to write the blocks of the subharmonic time-dependent Koopman-Hill projection matrix  $\tilde{\mathbf{Q}}(t) = e^{i\tilde{\omega}\tilde{\mathbf{D}}t} e^{\tilde{\mathbf{H}}t} \tilde{\mathbf{W}}$  in sum formulation according to Theorem 4:

$$\tilde{\mathbf{Q}}_{\tilde{j}}(t) = \mathbf{I} + \sum_{m=1}^{\infty} \sum_{\tilde{\mathbf{p}} \in \tilde{\mathcal{P}}_{\tilde{j}}^{(m)}} \tilde{\xi}_{\tilde{\mathbf{p}}}(t) \tilde{\mathcal{J}}_{\tilde{\mathbf{p}}} = \mathbf{I} + \sum_{m=1}^{\infty} \sum_{\mathbf{p} \in \mathcal{P}_{\frac{\tilde{j}}{2}}^{(m)}} \xi_{\mathbf{p}}(t) \mathcal{J}_{\mathbf{p}} \quad \tilde{j} = -2N, \dots, 2N. \quad (101)$$

The series (101) is very similar to the series (78) for the direct Koopman-Hill projection, but the index of the summation set  $\mathcal{P}^{(m)}$  on the right-hand side can now additionally admit values that are not integer. To understand the significance of the sets  $\mathcal{P}_{\frac{j}{2}}^{(m)}$  for non-integer index, it is beneficial to consider a bijection that maps these sets to hypercubes in  $\mathbb{Z}^m$ .

**Lemma 7** (Identification of the set  $\mathcal{P}_j^{(m)}$  with a hypercube). *For  $m \in \mathbb{N}$  and  $j \in \mathbb{R}$ , let*

$$\mathcal{Q}_j^{(m)} := \{ \mathbf{q} \in \mathbb{Z}^m : |q_k - j| \leq N \text{ for all } k = 1, \dots, m \} = \{ [j - N], \dots, [j + N] \}^m \quad (102)$$

denote the set of all integer tuples located inside the hypercube of edge length  $2N$ , centered around  $(j, \dots, j) \in \mathbb{R}^m$ . Here,  $\lceil \cdot \rceil$  and  $\lfloor \cdot \rfloor$  denote the *ceil* and *floor* operations, respectively. The function  $\boldsymbol{\rho} : \mathbb{Z}^m \rightarrow \mathbb{Z}^m$ ,  $\mathbf{q} \mapsto \mathbf{p}$  with  $p_1 = q_1$  and  $p_k = q_k - q_{k-1}$ ,  $k = 2, \dots, m$ , provides a bijection from the set  $\mathcal{Q}_j^{(m)}$  onto the set  $\mathcal{P}_j^{(m)}$ .

*Proof.* The right-hand side of (102) follows directly from the conditions  $q_k \leq N + j$  and  $-q_k \leq N - j$  for each individual  $k$ . The function  $\boldsymbol{\rho}$  is bijective on  $\mathbb{Z}^m$  with  $q_k = \sum_{i=1}^k p_i$  for  $k = 1, \dots, m$ . The bijection follows by substituting  $q_k = \sum_{i=1}^k p_i$  in (102).  $\square$

If  $j$  is integer, then both the lower and upper bound in (102) are admitted and  $\mathcal{Q}_j^{(m)}$  has  $(2N + 1)^m$  elements, cf. Figs. 5a and 5b. Otherwise, the lower and upper bound are both rounded towards zero and  $\mathcal{Q}_j^{(m)}$  only has  $(2N)^m$  entries, cf. Figs. 5d and 5e. Geometrically, the function  $\boldsymbol{\rho}$  skews the hypercube around the point  $(0, \dots, 0)$  in all directions except  $q_1$  to arrive at a parallelotope. For  $m = 2$ , this process is illustrated in Figures 5c and 5f.

We are now ready to formulate the series representation of the corresponding subharmonic Koopman-Hill projection, expressed in the original non-subharmonic Fourier coefficients.

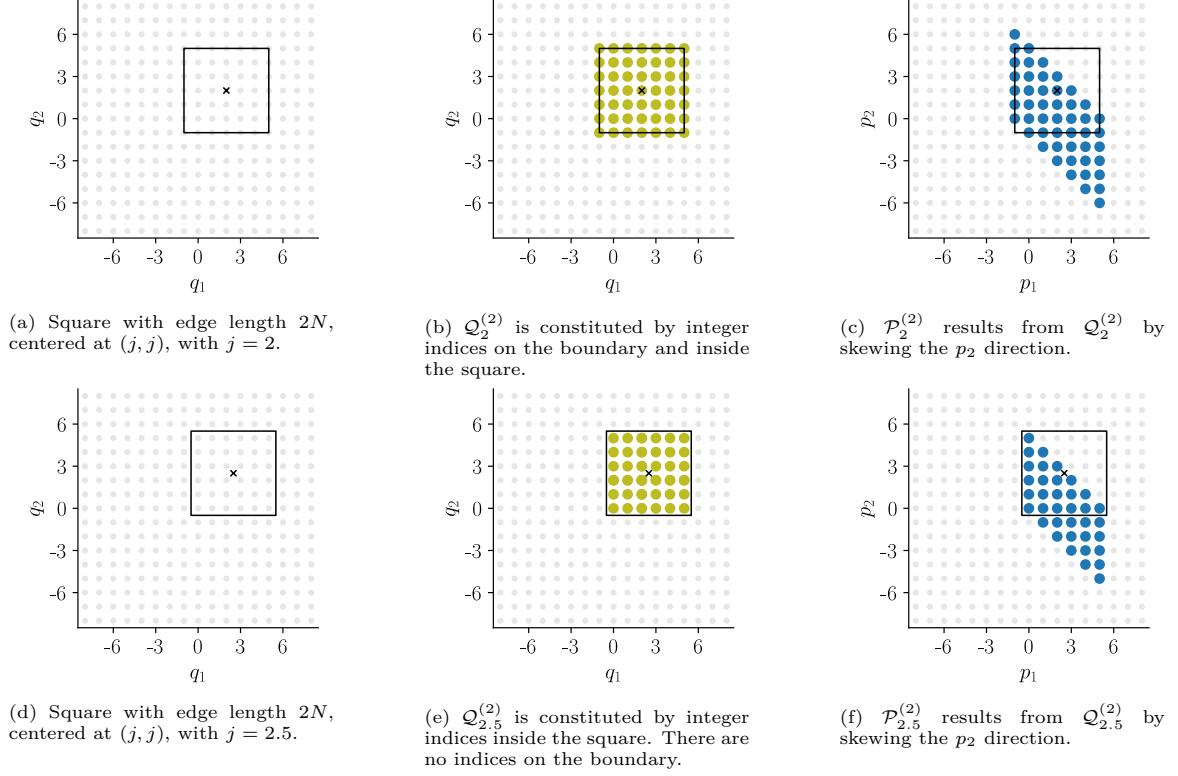


Figure 5: Flowchart illustrating the bijection between sets  $\mathcal{Q}_j^{(2)}$  and  $\mathcal{P}_j^{(2)}$  for  $j = 2$  ((a) – (c)) and  $j = 2.5$  ((d) – (f)).

**Theorem 8** (Series expression for  $\Phi_{\text{subh}}$ ). *The series expression for the subharmonic Koopman-Hill projection formulation (91) is given by*

$$\tilde{\mathbf{C}}_{\text{subh}} e^{i\omega \tilde{\mathbf{D}} t} e^{\tilde{\mathbf{H}} t} \tilde{\mathbf{W}} = \tilde{\mathbf{C}}_{\text{subh}} \tilde{\mathbf{Q}}(t) = \mathbf{I} + \sum_{m=1}^{\infty} \sum_{\mathbf{p} \in \mathcal{P}_{\text{subh}}^{(m)}} \xi_{\mathbf{p}} \mathcal{J}_{\mathbf{p}} \quad (103)$$

with the integer index sets

$$\mathcal{P}_{\text{subh}}^{(m)} = \left\{ \mathbf{p} \in \mathbb{Z}^m : \left| \sum_{l=v}^w p_l \right| \leq 2N \text{ for all } v, w = 1, \dots, m \right\}. \quad (104)$$

The series converges absolutely for all  $t \in \mathbb{R}$ .

*Proof.* Using (101), the product  $\tilde{\mathbf{C}}_{\text{subh}} \tilde{\mathbf{Q}}(t)$  is given by

$$\Phi_{\text{subh}}(t) = \tilde{\mathbf{C}}_{\text{subh}} \tilde{\mathbf{Q}}(t) = \tilde{\mathbf{C}}_{\text{subh}} \tilde{\mathbf{W}} + \sum_{\tilde{j}=-2N}^{2N} (-1)^{\tilde{j}} \sum_{m=1}^{\infty} \sum_{\mathbf{p} \in \mathcal{P}_{\frac{\tilde{j}}{2}}^{(m)}} \xi_{\mathbf{p}}(t) \mathcal{J}_{\mathbf{p}}. \quad (105)$$

Due to the alternating sign of  $(-1)^{\tilde{j}}$ , values of  $\mathbf{p}$  that lie in the intersection of  $\mathcal{P}_j^{(m)}$  and  $\mathcal{P}_{j+\frac{1}{2}}^{(m)}$  cancel each other out. To see this more clearly, we look at the summands of (105) for one fixed  $m \in \mathbb{N} \setminus \{0\}$  and parameterize any set  $\mathcal{P}_j^{(m)}$  by its corresponding hypercube  $\mathcal{Q}_j^{(m)}$ :

$$\sum_{\tilde{j}=-2N}^{2N} \sum_{\mathbf{p} \in \mathcal{P}_{\frac{\tilde{j}}{2}}^{(m)}} (-1)^{\tilde{j}} \xi_{\mathbf{p}} \mathcal{J}_{\mathbf{p}} = \sum_{\mathbf{q} \in \mathcal{Q}_N^{(m)}} \xi_{\rho(\mathbf{q})} \mathcal{J}_{\rho(\mathbf{q})} + \sum_{j=-N}^{N-1} \left( \sum_{\mathbf{q} \in \mathcal{Q}_j^{(m)}} \xi_{\rho(\mathbf{q})} \mathcal{J}_{\rho(\mathbf{q})} - \sum_{\mathbf{q} \in \mathcal{Q}_{j+\frac{1}{2}}^{(m)}} \xi_{\rho(\mathbf{q})} \mathcal{J}_{\rho(\mathbf{q})} \right). \quad (106)$$

As  $j$  is integer, the hypercube  $\mathcal{Q}_{j+\frac{1}{2}}^{(m)}$  is a strict subset of the hypercube  $\mathcal{Q}_j^{(m)}$ , where the ceil operation of (102) is activated. Hence, the set difference between them is

$$\mathcal{Q}_j^{(m)} \setminus \mathcal{Q}_{j+\frac{1}{2}}^{(m)} = \{\mathbf{q} \in \mathbb{Z}^m \mid \exists k : q_k = j - N \text{ and } |q_w - j| \leq N \ \forall w = 1, \dots, m\}. \quad (107)$$

This set difference is visualized in Figure 6a for the case  $m = 2$ . As the centerpoint of the square shifts from  $-3$  to  $-2.5$ , the integer indices that were exactly at the boundary of the blue square, and thus contained in the set  $\mathcal{Q}_{-3}^{(2)}$ , are outside the olive square, corresponding to  $\mathcal{Q}_{-2.5}^{(m)}$ . The set difference between both these sets corresponds to two of the four edges of the blue square. Likewise, for  $m > 2$ , the set differences  $\mathcal{Q}_j^{(m)} \setminus \mathcal{Q}_{j+\frac{1}{2}}^{(m)}$  correspond to  $(m - 1)$ -dimensional sides of the  $m$ -hypercube. They are disjoint for distinct integer values of  $j$ . Using these arguments and  $\mathbf{C}_{\text{subh}} \tilde{\mathbf{W}} = \mathbf{I}$  in (105), the subharmonic projection

$$\Phi_{\text{subh}}(t) = \mathbf{I} + \sum_{m=1}^{\infty} \sum_{\mathbf{q} \in \mathcal{Q}_{\text{subh}}^{(m)}} \xi_{\rho(\mathbf{q})}(t) \mathbf{J}_{\rho(\mathbf{q})} \quad (108)$$

is given by summation over the union

$$\mathcal{Q}_{\text{subh}}^{(m)} = \bigcup_{j=-N}^{N-1} \left( \mathcal{Q}_j^{(m)} \setminus \mathcal{Q}_{j+\frac{1}{2}}^{(m)} \right) \cup \mathcal{Q}_N^{(m)} \quad (109)$$

of all the disjoint set differences with the remaining set  $\mathcal{Q}_N$ . Equivalently, one can leave the set  $\mathcal{Q}_0^{(m)}$  intact and consider the upper sides of the hypercubes for  $j > 0$ , instead of the lower ones :

$$\mathcal{Q}_{\text{subh}}^{(m)} = \mathcal{Q}_0^{(m)} \cup \bigcup_{j=1}^N \left( \mathcal{Q}_j^{(m)} \setminus \mathcal{Q}_{j-\frac{1}{2}}^{(m)} \right) \cup \left( \mathcal{Q}_{-j}^{(m)} \setminus \mathcal{Q}_{-j+\frac{1}{2}}^{(m)} \right). \quad (110)$$

This union of set differences is visualized in Figure 6b for  $m = 2$ . The corresponding set  $\mathcal{P}_{\text{subh}}^{(2)}$ , where every index is skewed by the bijection  $\rho$  of Lemma 7, is visualized in Figure 6c.

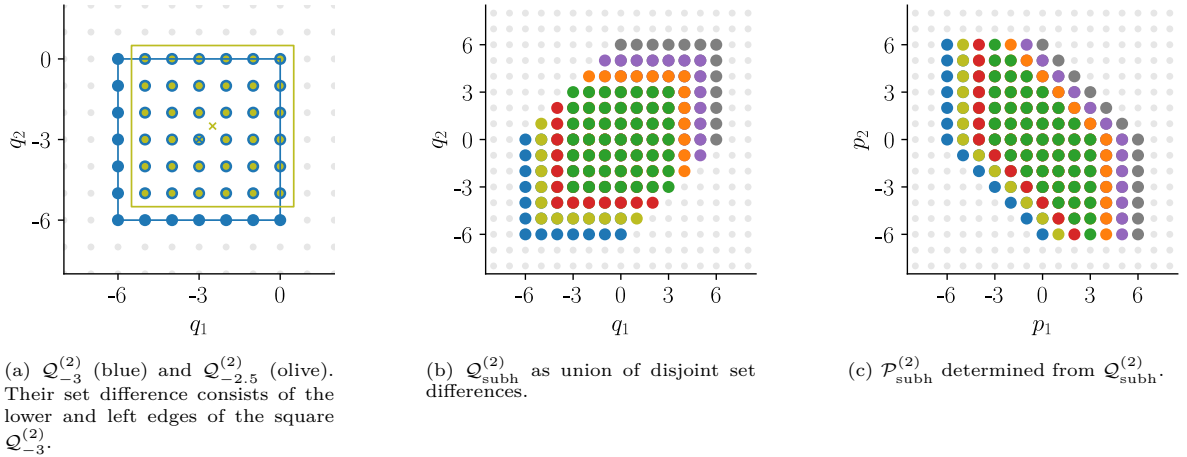


Figure 6: Visualization for the construction of sets  $\mathcal{Q}_{\text{subh}}^{(2)}$  and  $\mathcal{P}_{\text{subh}}^{(2)}$  for  $N = 3$ .

As any set  $\mathcal{Q}_{j+\frac{1}{2}}^{(m)}$  is a strict subset of  $\mathcal{Q}_{j+1}^{(m)}$  as well as of  $\mathcal{Q}_j^{(m)}$ , we may equivalently describe  $\mathcal{Q}_{\text{subh}}^{(m)}$  as a union of overlapping sets

$$\mathcal{Q}_{\text{subh}}^{(m)} = \bigcup_{j=-N}^N \mathcal{Q}_j^{(m)} = \{\mathbf{q} \in \mathbb{Z}^m \mid \exists j \in \{-N, \dots, N\} : |j - q_k| \leq N \text{ for all } k = 1, \dots, m\}. \quad (112)$$

In particular, it follows that every set  $\mathcal{P}_j^{(m)}$  of the direct projection is a strict subset of  $\mathcal{P}_{\text{subh}}^{(m)}$ . To complete the proof, it remains to show that this union of sets is also described by

$$\hat{\mathcal{Q}}_{\text{subh}}^{(m)} := \{\mathbf{q} \in \mathbb{Z}^m : |q_k| \leq 2N \text{ and } |q_k - q_w| \leq 2N \text{ for all } k, w = 1, \dots, m\}, \quad (113)$$

which is the bijection of the set (104). First, consider  $\mathbf{q} \in \mathcal{Q}_{\text{subh}}^{(m)}$ . There exists (at least one)  $j \in \{-N, \dots, N\}$  such that  $\mathbf{q}$  lies within the corresponding hypercube  $\mathcal{Q}_j^{(m)}$ . By the definition of the hypercube, it holds that  $j - N \leq q_k \leq j + N$  for all  $k = 1, \dots, m$  with this same fixed  $j$ . From  $|j| \leq N$  we immediately get  $|q_k| \leq 2N$ . For arbitrary  $w, k \in \{1, \dots, m\}$ , we can also build the inequalities

$$q_w - q_k \geq j - N - (j + N) = -2N \quad (114a)$$

$$q_w - q_k \leq j + N - (j - N) = 2N \quad (114b)$$

and therefore  $\hat{\mathcal{Q}}_{\text{subh}}^{(m)}$  is a subset of  $\mathcal{Q}_{\text{subh}}^{(m)}$ . For the inverse direction, consider  $\mathbf{q} \in \hat{\mathcal{Q}}_{\text{subh}}^{(m)}$ . We must find  $j \in \{-N, \dots, N\}$  such that  $\mathbf{q} \in \mathcal{Q}_j^{(m)}$ . To this end, we define the maximum and minimum values of  $\mathbf{q}$  as

$$q_{\max} := \max_w q_w \leq 2N \quad q_{\min} := \min_w q_w \geq -2N. \quad (115)$$

Definition (113) ensures that  $q_{\max} - q_{\min} \leq 2N$ . If  $q_{\min} \geq 0$ , we choose  $j = N$ . Then, the bounds

$$-N \leq q_{\min} - j \leq q_k - j \leq 2N - N \quad (116)$$

ensure that all  $q_k$  fulfill  $|q_k - j| \leq N$  and, thus,  $\mathbf{q} \in \mathcal{Q}_N^{(m)}$  holds. Otherwise, if  $q_{\min} < 0$ , we choose  $j = q_{\min} + N$ . Then, the bounding sequence is

$$-N = q_{\min} - j \leq q_k - j \leq q_{\max} - j = (q_{\max} - q_{\min}) - (j - q_{\min}) \leq 2N - N, \quad (117)$$

which guarantees  $\mathbf{q} \in \mathcal{Q}_{q_{\min} + N}^{(m)}$ . In summary, as the sets  $\mathcal{Q}_{\text{subh}}$  and  $\hat{\mathcal{Q}}_{\text{subh}}$  are both subsets of each other, they must be equal.  $\square$

#### 6.4. Convergence of the subharmonic formulation

In this section, we analyze the convergence of the subharmonic Koopman-Hill projection using its series expression (103) and the tools of the previous sections. As in Section (5), we want to bound

$$\tilde{\mathbf{E}}(t) = \Phi(t) - \tilde{\mathcal{C}}_{\text{subh}} e^{i\omega \tilde{\mathbf{D}} t} e^{\tilde{\mathbf{H}} t} \tilde{\mathbf{W}} = \sum_{m=1}^{\infty} \sum_{\mathbf{p} \in \mathbb{Z}^m \setminus \mathcal{P}_{\text{subh}}^{(m)}} \xi_{\mathbf{p}}(t) \mathcal{J}_{\mathbf{p}}. \quad (118)$$

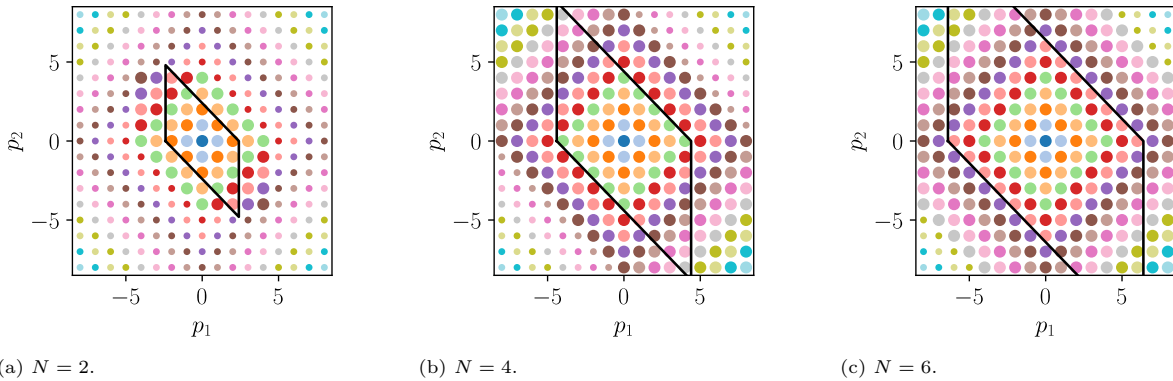


Figure 7: Visualization of 1-norm and integer index set  $\mathcal{P}_{\text{subh}}^{(2)}$  for the subharmonic projection. Dots of equal color have equal 1-norm. Large dots are elements of  $\mathcal{P}_{\text{subh}}^{(2)}$  with the chosen truncation order. Boundary of  $\mathcal{P}_0^{(2)}$  is visualized by black line.

Analogously to Figure 4, Figure 7 shows the sets  $\mathcal{P}_{\text{subh}}^{(2)}$  for different truncation orders  $N$  as large dots. Integer index tuples that are not represented in  $\mathcal{P}_{\text{subh}}^{(2)}$  are visualized as small dots and dots of equal color have

equal 1-norm. For reference, the outline of the set  $\mathcal{P}_0^{(m)}$  of the direct projection is indicated by a black line. In the figures, the largest rhombus that is contained within  $\mathcal{P}_{\text{subh}}$  is of size  $2N$ , twice as large as in the direct projection. This also follows immediately from the definition (104) as  $|\sum_{l=v}^w p_l| \leq |\mathbf{p}|$ . The rhombus is twice as large as the corresponding rhombus for the direct projection. Hence, we can repeat the bounding steps of Section 5, but with the rhombus size  $N$  replaced by  $2N$ , to arrive at the analogous error bound, formulated in the following theorem.

**Theorem 9** (Convergence and error bound of the subharmonic Koopman-Hill projection). *Let Assumption 1 hold. For  $b > \ln 2$  and for a fixed truncation order  $N \in \mathbb{N}$ , the approximation error between the true fundamental solution matrix and the subharmonic Koopman-Hill projection (91) is bounded by*

$$\left\| \Phi(t) - \tilde{\mathbf{C}}_{\text{subh}} e^{i\omega \tilde{\mathbf{D}}t} e^{\tilde{\mathbf{H}}t} \tilde{\mathbf{W}} \right\| \leq (2e^{-b})^{2N} e^{|4at|}. \quad (119)$$

*This error bound decays exponentially with  $N$ , providing a convergence guarantee of the Koopman-Hill projection. Satisfaction of a desired accuracy  $\|\Phi(t) - \mathbf{C}e^{\mathbf{H}t}\mathbf{W}\| \leq E_{\text{des}}$  is guaranteed if the truncation order fulfills*

$$N \geq \tilde{N}^* = \frac{2at - \ln(\sqrt{E_{\text{des}}})}{b - \ln 2}. \quad (120)$$

*Remark.* The bound (119) decays exponentially at twice the rate as the corresponding bound (81) of the direct formulation. The required truncation order  $N$  is now governed by the square root of the desired error.

*Proof.* The proof follows by replacing  $N$  by  $2N$  in Equations (85) – (87) during the proof of Theorem 6.  $\square$

## 7. Examples and discussion

In this section, the abstract series representations of the main body are illustrated using two examples. First, the scalar example of Section 3 is revisited and analyzed using the notation of the main results. Afterwards, the Duffing oscillator is examined as a more realistic example.

### 7.1. Scalar example revisited

The scalar example of Section 3 was used to motivate the series representations containing monomials of the Fourier coefficients. While the general series expression (34) and the series expression (26) of the example share many characteristics, their summands are not identical. This is because the series expression (26) inherently uses structural knowledge about the system, i.e., commutativity of scalar Fourier coefficients and the fact that most Fourier coefficients are zero.

For the scalar dynamics (23),  $\mathcal{J}_{\mathbf{p}}$  is zero whenever  $\mathbf{p}$  contains any entry that is larger than 1 in magnitude. Hence, the summation over  $\mathbb{Z}^m$  in (34) can be restricted to the set  $\{-1, 0, 1\}^m$ . Consider such a  $\mathbf{p} \in \{-1, 0, 1\}^m$ . Entries  $p_k = 0$  refer to  $J_0 = \beta$ , while all other entries refer to  $J_1 = J_{-1} = \gamma$ . The number of nonzero entries is  $|\mathbf{p}|$  and, correspondingly, there are  $m - |\mathbf{p}|$  entries in  $\mathbf{p}$  that are zero. Hence, the product of Fourier coefficients is given by  $\mathcal{J}_{\mathbf{p}} = \beta^{(m-|\mathbf{p}|)}\gamma^{|\mathbf{p}|}$ . Substituting these insights into the general series expression (34) yields

$$\phi(t) = 1 + \sum_{m=1}^{\infty} \sum_{\mathbf{p} \in \{-1, 0, 1\}^m} \xi_{\mathbf{p}}(t) \beta^{(m-|\mathbf{p}|)} \gamma^{|\mathbf{p}|}. \quad (121)$$

The  $\gamma$  and  $\beta$  terms are only influenced by the magnitude of  $\mathbf{p}$  and not its actual value. As in the previous sections, we sum over this magnitude to obtain

$$\phi(t) = 1 + \sum_{m=1}^{\infty} \sum_{M=0}^m \left( \sum_{\substack{\mathbf{p} \in \{-1, 0, 1\}^m \\ |\mathbf{p}|=M}} \xi_{\mathbf{p}}(t) \right) \beta^{(m-M)} \gamma^M. \quad (122)$$

After swapping the sums and using the index shift  $l = m - M$ , we arrive at

$$\phi(t) = \sum_{M=0}^{\infty} \sum_{l=0}^{\infty} \left( \sum_{\substack{\mathbf{p} \in \{-1, 0, 1\}^{M+l} \\ |\mathbf{p}|=M}} \xi_{\mathbf{p}}(t) \right) \beta^l \gamma^M. \quad (123)$$



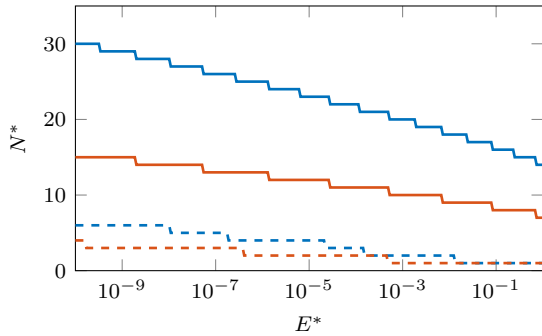
The comparison with (26) reveals the relationship

$$\hat{\xi}(l, k, t) = \sum_{\substack{\mathbf{p} \in \{-1, 0, 1\}^{l+k} \\ |\mathbf{p}|=k}} \xi_{\mathbf{p}}(t) = \frac{t^l (2 \sin t)^k}{(l+k)!} \quad (124)$$

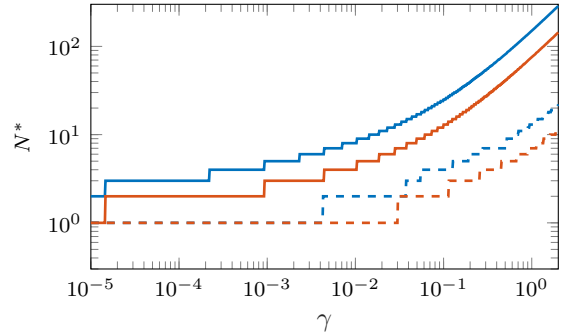
between the scalar factors. Below we discuss how this relationship confirms the observations made in Section 3.

A first observation was that the scalar factors are exactly met by the Koopman-Hill approximation for  $k = 0$ . As the multi-index  $\mathbf{p} = 0$ , which is the only one to fulfill  $|\mathbf{p}| = k = 0$ , is always contained in the index set  $\mathcal{P}_0^{(m)}$ , this is confirmed. Further, we observed numerically that the scalar factors are exactly met if  $k \leq N$ . This directly corresponds to the rhombus of integer indices with magnitude  $\leq N$  that is contained in the set  $\mathcal{P}_0^{(m)}$ , as discussed in Section 5.

Finally, we observed numerically that, for  $l > N$ , the scalar factors of the true fundamental solution and the Koopman-Hill approximation differ but are both nonzero. At first glance, this might seem to contradict the statement of Theorem 4, which asserts that all scalar factors of the Koopman-Hill approximation are either exactly those of the true fundamental solution or zero. However, (124) shows that the factor  $\hat{\xi}$  in the scalar example is composed of multiple scalar factors  $\xi_{\mathbf{p}}$ . For  $l > N$ , some of these factors will lie inside  $\mathcal{P}_0$  and others will not, resulting in a scalar factor  $\hat{\xi}$  that is nonzero but not exactly equal to the true fundamental solution.



(a)  $N^*$  (solid) and  $N_{\text{num}}$  (dashed) over  $E^*$  for  $\gamma = 0.1$  with direct (blue) and subharmonic (orange) Koopman-Hill projection.



(b)  $N^*$  (solid) and  $N_{\text{num}}$  (dashed) over  $\gamma$  for  $E^* = 10^{-6}$  with direct (blue) and subharmonic (orange) Koopman-Hill projection.

Figure 8: Guaranteed ( $N^*$ ) and actual ( $N_{\text{num}}$ ) truncation order needed to achieve a truncation error smaller than  $E^*$  for the example (23).

As the solution of the scalar example is available in closed form, the actual error of the Koopman-Hill approximation with a given  $N$  can be compared to the bound derived in Section 5. We make this comparison for the monodromy matrix, i.e., at  $t = T = 2\pi$ . To apply the error bound (81) of Theorem 6, explicit values for the exponential decay parameters  $a$  and  $b$  are needed. To make the bound (81) as small as possible, it is desirable to choose  $a$  as small as possible and  $b$  as large as possible. Due to the finite support of the Fourier coefficients,  $b$  can be chosen arbitrarily as  $b = \ln(2) - \ln(\varepsilon)$  with  $\varepsilon < 1$ . The minimal value of  $a$  that satisfies Assumption 1 is

$$a = \max \{ \beta, \gamma e^b \}. \quad (125)$$

We consider here only the more interesting case  $\gamma > 2\beta$  where the maximum is attained by the second option, i.e.,  $a = \frac{2\gamma}{\varepsilon}$ . Substituting these choices for  $a$  and  $b$  into the error bound (81) yields

$$|\mathbf{E}(T)| \leq \varepsilon^N \exp \left( 16\pi \frac{\gamma}{\varepsilon} \right) =: \varepsilon^N \exp \left( \zeta \frac{\gamma}{\varepsilon} \right) \quad (126)$$

where we introduced the abbreviation  $\zeta = 16\pi \approx 50$ . This error bound holds for all  $\varepsilon < 1$ . The value of  $\varepsilon$  that minimizes the bound (126) is  $\varepsilon^* = \frac{\zeta\gamma}{N}$ . Substituting  $\varepsilon^*$  back into (126) yields the best possible bound

$$E^* = \exp(N(1 + \ln(\zeta\gamma) - \ln(N))) = \left( \frac{\zeta\gamma}{N} \right)^N e^N. \quad (127)$$

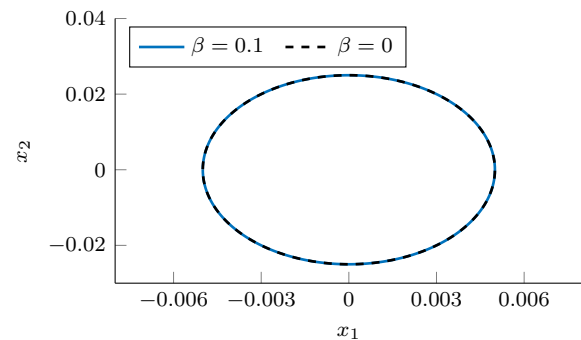
Table 1: Parameter values for Duffing oscillator.

Parameter	stiffnesses		damping	excitation		$\ \mathbf{J}_k\ $ decay	
	$\alpha$	$\beta$	$\delta$	$F$	$\omega$	$a$	$b$
Configuration 1	5	0.1	0.02	0.1	5	5.00	7.40
Configuration 2	0.5	3	0.05	0.1	0.3	6.74	1.12

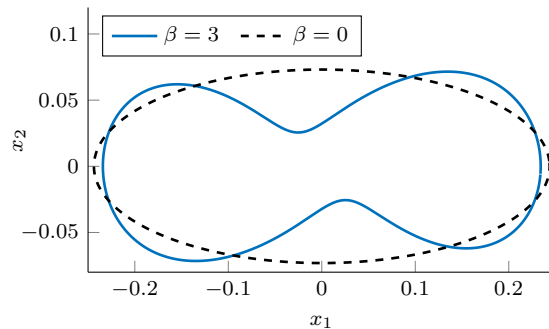
For a fixed  $\gamma$  and a desired accuracy  $E^*$ , we can numerically determine the required truncation order  $N^*$  to satisfy the error bound. Figure 8a illustrates this truncation order  $N^*$  across a range of desired errors for  $\gamma = 0.1$ . Figure 8b shows the truncation order  $N^*$  needed to ensure an error smaller than  $10^{-6}$  for various values of  $\gamma$ . Additionally, Figure 8b shows the smallest truncation order  $N$  that achieves an error smaller than  $10^{-6}$  for the direct Koopman-Hill projection against the true fundamental solution (24). This comparison is also made for the subharmonic approach.

It is immediately evident that the derived error bounds become rather conservative as  $\gamma$  increases. Even for this simple example, the required truncation order  $N^*$  to guarantee sufficiently small errors reaches  $N^* = 100$ , while the truncation order that is actually needed stays around  $N = 10$ . This discrepancy arises from the conservative bounding steps employed throughout this work to enable closed-form expressions of the series. Nevertheless, the subharmonic approach consistently requires approximately half the truncation order of the direct approach.

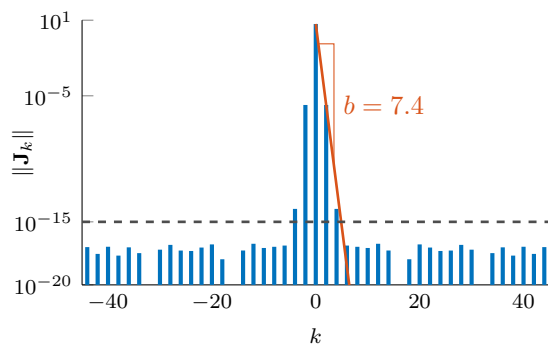
## 7.2. Duffing oscillator



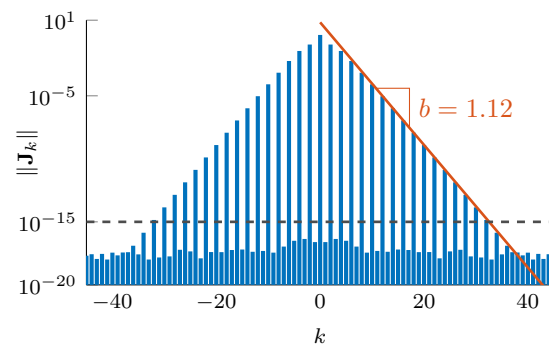
(a) Periodic solution in Configuration 1 (solid blue) and solution of the corresponding linear system (dashed black).



(b) Periodic solution in Configuration 2 (solid blue) and solution of the corresponding linear system (dashed black).



(c) Norm of the Fourier coefficient matrices in Configuration 1.



(d) Norm of the Fourier coefficient matrices in Configuration 2.

Figure 9: Periodic solutions for the two considered configurations of the Duffing oscillator and norm of Fourier coefficient matrices.

In this example, we consider the forced Duffing oscillator to showcase the applicability of the error bound to stability determination of periodic solutions. The considered forced Duffing oscillator in first-order form

and the corresponding system matrix for a perturbation around a solution  $\mathbf{x}(t)$  are

$$\dot{\mathbf{x}} = \mathbf{f}(\mathbf{x}) = \begin{pmatrix} x_2 \\ -\alpha x_1 - \beta x_1^3 - \delta x_2 + F \cos \omega t \end{pmatrix}, \quad \mathbf{J}(t) = \frac{\partial \mathbf{f}}{\partial \mathbf{x}} \Big|_{\mathbf{x}(t)} = \begin{pmatrix} 0 & 1 \\ -\alpha - 3\beta x_1(t)^2 & -\delta \end{pmatrix}. \quad (128)$$

We consider two parameter settings, detailed in Table 1.

The periodic solutions of the two configurations, depicted in Figure 9, were determined using the harmonic balance method with  $N = 45$  Fourier coefficients. Configuration 1, where the forcing frequency is well beyond the resonance frequency and the cubic stiffness is low, could be labeled as an almost-linear case where the periodic solution visually coincides with that of the corresponding linear system ( $\beta = 0$ , all other parameters as in Table 1), cf. Figure 9a. In Configuration 2, where the cubic stiffness is high and the forcing frequency is low, the higher-frequency components of the periodic solution due to the nonlinear effects are clearly visible in Figure 9b.

The exponential decay of the Fourier coefficients is analyzed in Figures 9c and 9d. Due to machine precision, only Fourier coefficient matrices with a numerically determined norm larger than  $10^{-15}$  have been taken into account to fit the exponential decay parameters  $a$  and  $b$ . The resulting parameters for both configurations are reported in Table 1.

Figure 10 shows in solid lines the truncation orders  $N^*$  that are expected to guarantee an error smaller than  $10^{-6}$  using the error bound (82). At each time  $t$ , the fundamental solution matrices obtained using (17a) with increasing truncation orders  $N$  were compared against a reference fundamental solution matrix obtained by integrating (2) from 0 to  $t$  using Matlab's `ode45` numerical integrator with absolute and relative tolerances set to  $10^{-10}$ . For every considered time sample  $t$ , the lowest value of  $N$  where the norm of the difference between these two fundamental matrices is lower than  $10^{-6}$  is reported in dashed lines in Figure 10.

As in the previous example, the error bound is not tight. In particular, the expected truncation orders  $N^*$  increase linearly with  $t$ , while the numerically determined truncation orders  $N_{\text{num}}$  do not. This renders the error bound overly conservative for larger  $t$ , especially if  $b$  is small.

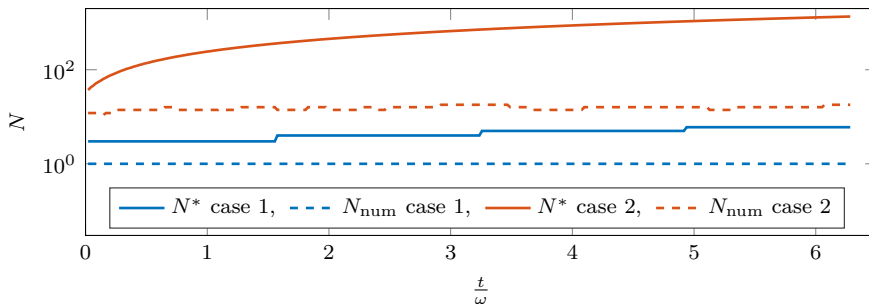


Figure 10: Truncation orders  $N$  needed to guarantee (solid) and numerically achieve (dashed) an error smaller than  $10^{-6}$  for the fundamental solution matrix of the Duffing oscillator.

## 8. Conclusion

In this paper, we provided a convergence proof and the explicit error bounds (81), (119) for the numerical computation of the fundamental solution matrix of an LTP system using two variants of the Koopman-Hill projection method. The proof relies on expressing both the fundamental solution matrix as well as its approximation as series and then comparing the summands. While the series expressions are well-defined for all time-periodic system matrices where the Fourier coefficients decay exponentially, the error bounds and thus the convergence proof are valid for systems where the decay rate is sufficiently large ( $b > \ln 2$ ).

Theorem 6 provides valuable theoretical backing for the use of the Hill matrix in the context of the harmonic balance method. Up until now, the only available convergence guarantee for any Hill-matrix-based method was in the context of the imaginary-part-based sorting method [11, Prop. 3]. While applicable to system matrices that are differentiable with piecewise continuous derivative, which is a larger system class than our proof, the proof of [11] does not come with an explicit error bound and gives no indication at all how to choose  $N$  to

be sufficiently large in practice. Thus, the error bound derived in the present work is the most explicit one available for all Hill matrix approaches and provides a helpful justification for the practitioner with an upper bound on the required truncation order  $N$ .

The examples of Section 7.2 show that the error bound is conservative and overestimates the required truncation order  $N$ . This conservatism arises from the bounding steps employed to enable closed-form expressions of the series. Specifically, to upperbound the number of index tuples with a given 1-norm in the series for the error, *all* integer index tuples that do not lie in the largest rhombus within  $\mathcal{P}_0^{(m)}$  (or  $\mathcal{P}_{\text{subh}}^{(m)}$ ) were counted, irrespective of whether they actually lie inside  $\mathcal{P}_0^{(m)}$  (resp.  $\mathcal{P}_{\text{subh}}^{(m)}$ ) or not. The ratio of tuples in this rhombus over all tuples in  $\mathcal{P}_0^{(m)}$  or  $\mathcal{P}_{\text{subh}}^{(m)}$  goes to zero as  $m$  grows. Hence, especially for large  $m$ , our error bound includes significantly more summands than necessary, contributing to overly conservative convergence requirements. Furthermore, the error bound depends exponentially on the time  $t$  and on the decay parameter  $a$ . However, the numerical results do not indicate any dependence on time at all. Potentially, a tighter bound independent of  $t$  could be derived by exploiting the periodicity of the scalar factors or finding a better method to count only those scalar factors that actually lie outside  $\mathcal{P}$ . Additionally, summing from 0 to  $N + m$  instead of 1 to  $m$  in the final step of the convergence proof is required to eliminate the sum over the binomial coefficient but becomes more conservative as  $N$  increases. This summation produces the factor  $2^N$ , which leads to the term  $\ln 2$  in the convergence requirement  $b > \ln 2$  of Theorem 6. A tighter simplification of this summation could potentially remove  $\ln 2$  from the requirement. Similarly, algebraic simplifications like  $\left(\frac{x}{1-x}\right)^m < 1$  and  $\binom{N+m+1}{m}^{-1} < 1$  in the proof of Lemma 13 also become more conservative as  $m$  and  $N$  grow. For these reasons, we postulate that a similar bound to (81), but independent of  $t$  and applicable whenever Assumption 1 is satisfied, is likely to exist. This would make the result tighter and applicable to all analytic linear periodic differential equations. Further work is needed to derive such a bound.

This paper focused solely on the error caused by truncation of the Hill matrix. In practice, all involved operations are executed with finite machine precision on a computer. The error due to numerical procedures, in particular the error of evaluating the matrix exponential, is not considered in the error bound (81). However, the accurate numerical evaluation of matrix exponentials has been well researched [32–34], so the error due to the finite-precision procedures is expected to be negligible compared to the truncation error in practical applications.

## Appendix A. Combinatorics

This section and the following one collect some particular equivalences that are needed to handle the various series expressions occurring in this work. Some of these results are well-known and revisited here for the sake of completeness, while others are rather specific. We begin by stating a well-known result on the number of multi-indices with a given 1-norm.

**Lemma 10** (Stars and bars [35]).

- i) The set  $\{\boldsymbol{\alpha} \in \mathbb{N}^m : |\boldsymbol{\alpha}| = M\}$  has exactly  $\binom{M+m-1}{m-1}$  elements.
- ii) The set  $\{\mathbf{p} \in \mathbb{Z}^m : |\mathbf{p}| = M\}$  has fewer than  $2^m \binom{M+m-1}{m-1}$  elements.

*Proof.* Proposition i) is a classical combinatorics result that can be found, e.g., in [35]. For any nonnegative tuple  $\boldsymbol{\alpha} \in \mathbb{N}$  there are at most  $2^m$  tuples  $\mathbf{p} \in \mathbb{Z}$  which fulfill  $|p_k| = \alpha_k$  for all  $k = 1, \dots, m$  as every entry can be either positive or negative (yielding two independent options for each of the  $m$  entries), except if it is zero. This immediately proves Proposition ii).  $\square$

Next, we provide here a variant of Vandermonde’s identity [35] with the summation index in the upper entries, which enables a corollary about summation over multiple indices.

**Lemma 11.** For arbitrary  $n, M, P \in \mathbb{N}$ , the following expression holds:

$$\sum_{\alpha=0}^M \binom{\alpha+n}{n} \binom{M+P-\alpha}{M-\alpha} = \binom{M+P+n+1}{M}. \quad (\text{A.1})$$

*Proof.* This proof follows a classical counting argument. Consider the set  $\mathcal{D} := \{1, \dots, M + P + n + 1\}$ , which contains all strictly positive natural numbers up to  $M + P + n + 1$ . The number of subsets of the form  $\mathcal{A} := \{a_1, \dots, a_{P+n+1}\} \subset \mathcal{D}$  with  $P + n + 1$  unique elements  $a_1 < a_2 < \dots < a_{P+n+1}$  is  $\binom{M+P+n+1}{P+n+1} = \binom{M+P+n+1}{M}$ , which is the right-hand side of (A.1).

For the left-hand side, we construct another way to count these subsets. The  $(n+1)$ -th element  $a_{n+1}$  must have a value between  $n+1$  (implying  $a_k = k$  for the  $n$  elements  $a_k$  with  $k < n+1$ ) and  $n+1+M$  (implying  $a_k = M+k$  for the  $P$  elements with  $k > n+1$ ). Suppose that  $a_{n+1} = n+1 + \alpha$  for some  $\alpha \in \{0, \dots, M\}$ . As the elements before  $a_{n+1}$  must have smaller value and the elements after must have larger value, these subsets of  $\mathcal{A}$  must fulfill

$$\mathcal{A}_- := \{a_1, \dots, a_n\} \subset \{1, \dots, n + \alpha\} \quad (\text{A.2})$$

$$\mathcal{A}_+ := \{a_{n+2}, \dots, a_{n+P+1}\} \subset \{n + \alpha + 2, \dots, M + P + n + 1\}. \quad (\text{A.3})$$

Hence, for  $\mathcal{A}_-$  we choose  $n$  out of  $n + \alpha$  values, while for  $\mathcal{A}_+$  we choose  $P$  out of  $M + P - \alpha$  values. In summary, for every fixed  $\alpha$  there are  $\binom{n+\alpha}{n} \binom{M+P-\alpha}{P} = \binom{n+\alpha}{n} \binom{M+P-\alpha}{M-\alpha}$  subsets  $\mathcal{A}$  where  $a_{n+1} = n + 1 + \alpha$ , and summing over all possible values of  $\alpha$  completes the proof.  $\square$

This lemma enables a follow-up statement that deals with multiple sums.

**Lemma 12.** *For arbitrary  $M \in \mathbb{N}$ ,  $m \in \mathbb{N} \setminus \{0\}$  and  $\mathbf{n} = [n_1, \dots, n_m] \in \mathbb{N}^m$ , the following expression given by  $m$  finite-length sums holds:*

$$\sum_{\alpha_1=0}^M \sum_{\alpha_2=0}^{M-\alpha_1} \dots \sum_{\alpha_m=0}^{M-\alpha_1-\dots-\alpha_{m-1}} \binom{\alpha_1 + n_1}{n_1} \dots \binom{\alpha_m + n_m}{n_m} = \binom{m + M + |\mathbf{n}|}{M}. \quad (\text{A.4})$$

*Proof.* We prove this statement using Lemma 11 and complete induction.

*Base case  $m = 1$ .* The base case is covered immediately by Lemma 11 with  $P = 0$ .

*Induction assumption.* Assume that Corollary 12 holds for the case  $m - 1$ , i.e. for  $m - 1$  summation symbols. By increasing the index of all  $\alpha_i$  and  $n_i$  by 1 and replacing  $M$  by  $M - \alpha_1$  for arbitrary  $\alpha_1$  and  $M \geq \alpha_1$ , we can rewrite the induction assumption as

$$\sum_{\alpha_2=0}^{M-\alpha_1} \dots \sum_{\alpha_m=0}^{M-\alpha_1-\dots-\alpha_{m-1}} \binom{\alpha_2 + n_2}{n_2} \dots \binom{\alpha_m + n_m}{n_m} = \binom{(m-1) + (M - \alpha_1) + n_2 + \dots + n_m}{M - \alpha_1}. \quad (\text{A.5})$$

*Induction step.* In (A.4), the first binomial coefficient depends only on  $\alpha_1$  and can be pulled outside of the sums over  $\alpha_2, \dots, \alpha_m$ . Afterwards, the induction assumption (A.5) can be identified in the inner sums and the statement left to prove is

$$\sum_{\alpha_1=0}^M \binom{\alpha_1 + n_1}{n_1} \binom{m-1 + M - \alpha_1 + n_2 + \dots + n_m}{M - \alpha_1} = \binom{m + M + |\mathbf{n}|}{M}. \quad (\text{A.6})$$

As this statement is covered by Lemma 11 with  $P = m - 1 + n_2 + \dots + n_m$ , the proof is complete.  $\square$

## Appendix B. Taylor series of $(1 - x)^{-(1+k)}$

The following power series plays a central role in the construction of the series expressions and also in the convergence proof.

**Lemma 13.** *For arbitrary  $k \in \mathbb{N}$ ,  $q \in \mathbb{R}$  with  $q \geq 0$ , the power series*

$$\sum_{M=0}^{\infty} \binom{M+k}{k} M^q x^M \quad (\text{B.1})$$

converges absolutely if  $|x| < 1$ . In the case  $q = 0$ , the series has the closed-form expression

$$\sum_{M=0}^{\infty} \binom{M+k}{k} x^M = (1-x)^{-(1+k)} =: g(x). \quad (\text{B.2})$$

The Taylor remainder for a Taylor polynomial of degree  $N$  of this series is given by

$$R_N(x) := \sum_{M=N+1}^{\infty} \binom{M+k}{k} x^M = x^N \left( \sum_{m=0}^k \binom{N+k+1}{N+m+1} \left( \frac{x}{1-x} \right)^{m+1} \right). \quad (\text{B.3})$$

*Proof.* Denote summands of (B.1) by  $a_M$ . The quotient criterion yields

$$\lim_{M \rightarrow \infty} \left| \frac{a_{M+1}}{a_M} \right| = \lim_{M \rightarrow \infty} \frac{M+k+1}{M+k} \left( \frac{M+1}{M} \right)^q |x| = |x|, \quad (\text{B.4})$$

proving absolute convergence for  $|x| < 1$  and  $q \geq 0$ . For the special case  $q = 0$ , a straightforward induction procedure shows that the  $M$ -th derivative of  $g(x) = (1-x)^{-(1+k)}$  is

$$g^{(M)}(x) := \frac{d^M}{dx^M} (1-x)^{-(1+k)} = \frac{(M+k)!}{k!} (1-x)^{-(M+k+1)} \quad \text{for all } M \in \mathbb{N}. \quad (\text{B.5})$$

Evaluated at zero, these derivatives define the Taylor formula

$$g(x) = (1-x)^{-(k+1)} = \sum_{M=0}^N \frac{(M+k)!}{k!} \frac{x^M}{M!} + R_N(x), \quad (\text{B.6})$$

where  $N \in \mathbb{N}$  is the maximum degree of the Taylor polynomial and  $R_N(x)$  is the remainder.

The Taylor remainder in integral form [36] is given by

$$R_N(x) = \int_0^x \frac{(x-\tau)^N}{N!} g^{(N+1)}(\tau) d\tau = \int_0^x \frac{(x-\tau)^N}{N!} \frac{(N+1+k)!}{k!} (1-\tau)^{-(2+k+N)} d\tau. \quad (\text{B.7})$$

The substitution  $u = (1-\tau)^{-1}$  of the integration variable simplifies this integral to

$$R_N(x) = \int_1^{(1-x)^{-1}} \frac{u^k}{k!} \frac{(N+k+1)!}{N!} (1-(1-x)u)^N du, \quad (\text{B.8})$$

which is an integral over a polynomial in  $u$ . We evaluate this integral using  $(k+1)$ -times repeated integration by parts. The integrand of (B.8) is given by the product of the functions

$$v^{(0)}(u) := \frac{u^k}{k!} \quad (\text{B.9})$$

$$W^{(0)}(u) := \frac{(N+k+1)!}{N!} (1-(1-x)u)^N. \quad (\text{B.10})$$

For  $v$ , we can immediately compute its  $m$ -th derivatives

$$v^{(m)}(u) := \frac{d^m}{du^m} v^{(0)}(u) = \frac{u^{k-m}}{(k-m)!} \quad m = 0, \dots, k \quad (\text{B.11})$$

and the  $(k+1)$ -th derivative is zero. The function  $W^{(0)}$  has the  $m$ -th antiderivative

$$W^{(m)}(u) := (x-1)^{-m} \frac{(N+k+1)!}{(N+m)!} (1-(1-x)u)^{N+m} \quad (\text{B.12})$$

such that  $\frac{d^m}{du^m} W^{(m)}(u) = W^{(0)}(u)$  for  $m = 0, \dots, k+1$ . Performing  $k+1$  times the integration by parts on (B.8), each time using the next derivative of  $v$  and the next antiderivative of  $W$ , yields the formula

$$\int_1^{(1-x)^{-1}} v^{(0)} W^{(0)} du = \sum_{m=0}^k (-1)^m \left[ W^{(m+1)} v^{(m)} \right]_1^{(1-x)^{-1}} + (-1)^{k+1} \int_1^{(1-x)^{-1}} W^{(k+1)} v^{(k+1)} du, \quad (\text{B.13})$$

where the dependence on  $u$  was omitted for the sake of brevity. The integral on the right-hand side of (B.13) vanishes together with  $v^{(k+1)}$ , and each summand of the remaining boundary terms can be evaluated individually to

$$\begin{aligned} (-1)^m \left[ W^{(m+1)} v^{(m)} \right]_1^{(1-x)^{-1}} &= \left[ -(1-x)^{-(m+1)} \frac{(N+k+1)!}{(N+m+1)!(k-m)!} (1-(1-x)u)^{N+m+1} u^{k-m} \right]_1^{(1-x)^{-1}} \\ &= x^N \left( \frac{x}{1-x} \right)^{m+1} \binom{N+k+1}{N+m+1}. \end{aligned} \quad (\text{B.14})$$

Substituting (B.14) into (B.13) yields the desired expression (B.3) for the remainder.

To show that the remainder converges to zero as  $N \rightarrow \infty$ , we will proceed to bound the expression (B.3) from above. To lighten notation, we assume w.l.o.g that  $x > 0$  (otherwise, replace  $x$  by  $|x|$  and  $R_N(x)$  by  $|R_N(x)|$  in the developments below). From the factorial expressions it is easy to see that

$$\binom{N+k+1}{N+m+1} = \binom{N+k+1}{N+1} \binom{k}{m} \binom{N+m+1}{m}^{-1}. \quad (\text{B.15})$$

Noting that  $\binom{N+m+1}{m}^{-1} \leq 1$  for all  $m \in \mathbb{N}$ , we substitute (B.15) into the remainder (B.3) and use the binomial theorem to obtain

$$\begin{aligned} R_N(x) &\leq x^N \frac{x}{1-x} \binom{N+k+1}{N+1} \sum_{m=0}^k \binom{k}{m} \left( \frac{x}{1-x} \right)^m 1^{k-m} \\ &= \frac{x^{N+1}}{(1-x)} \binom{N+k+1}{N+1} \left( \frac{x}{1-x} + 1 \right)^k \\ &= \frac{x^{N+1}}{(1-x)^{k+1}} \binom{N+k+1}{N+1}. \end{aligned} \quad (\text{B.16})$$

Finally, using the bound  $\binom{N+1+k}{k} \leq (N+1)^{k+1}$ , we find for any fixed  $k \in \mathbb{N}$

$$0 \leq \lim_{N \rightarrow \infty} R_N(x) \leq \lim_{N \rightarrow \infty} x^{N+1} \left( \frac{N+1}{1-x} \right)^{k+1} = 0, \quad (\text{B.17})$$

completing the proof.  $\square$

### Appendix C. Periodicity of the scalar factor

An observation that can be drawn from the scalar example of Section 3 and from Figure 2 is that the scalar factor  $\xi_{\mathbf{p}}(t)$  has periodic components, possibly multiplied by a monomial in  $t$ . We show here that for most values of  $\mathbf{p}$ , indeed, this monomial vanishes and  $\xi_{\mathbf{p}}(t)$  is  $T$ -periodic.

**Theorem 14** (sufficient criterion for  $T$ -periodicity of  $\xi_{\mathbf{p}}$ ). *Let  $m \in \mathbb{N} \setminus \{0\}$  and consider an integer index tuple  $\mathbf{p} = [p_1, \dots, p_m] \in \mathbb{Z}^m$  which fulfills  $\sum_{l=v}^w p_l \neq 0$  for all  $v, w = 1, \dots, m$ . Then, the function  $\xi_{\mathbf{p}}$  is  $T$ -periodic and has a Fourier series  $\xi_{\mathbf{p}}(t) =: \sum_{k=-|\mathbf{p}|}^{|\mathbf{p}|} \xi_{\mathbf{p}}^{(k)} e^{ik\omega t}$  with finite support. In particular, the  $k$ -th Fourier coefficient  $\xi_{\mathbf{p}}^{(k)}$  can only be nonzero if  $k = 0$  or if there exists a  $w \in \{1, \dots, m\}$  such that  $k = \sum_{l=1}^w p_l$ .*

*Proof.* We prove this by induction.

*Base case  $m = 1$ .* Integrating the first statement of Lemma 3 for an arbitrary  $p \in \mathbb{Z} \setminus \{0\}$  with  $\xi_p(0) = 0$  yields

$$\xi_p(t) = \frac{1}{i\omega p} (e^{i\omega p t} - 1). \quad (\text{C.1})$$

In particular,  $\xi_p(t)$  is  $T$ -periodic and only the 0-th and  $p$ -th Fourier coefficient are nonzero.

*Induction assumption.* Let  $m \geq 2$ . Consider an integer index tuple  $\mathbf{p} = [p_1, p_2, \dots, p_m] \in \mathbb{Z}^m$  fulfilling the conditions of the theorem. The tuple  $[p_2, \dots, p_m] \in \mathbb{Z}^{m-1}$  fulfills the conditions of the theorem as well. The induction assumption is that  $\xi_{[p_2, \dots, p_m]}(t)$  is  $T$ -periodic and its Fourier coefficients  $\xi_{[p_2, \dots, p_m]}^{(k)}$  are only nonzero if  $k = 0$  or if there exists a  $w$  such that  $k = \sum_{l=2}^w p_l$ .

*Induction step.* Using the induction assumption, the second statement of Lemma 3, and the initial condition  $\xi_{\mathbf{p}}(0) = 0$ ,  $\xi_{\mathbf{p}}$  can be expressed by

$$\xi_{\mathbf{p}}(t) = \int_0^t \xi_{[p_2, \dots, p_m]}(\tau) e^{i\omega p_1 \tau} d\tau = \int_0^t \sum_{k=-|\mathbf{p}|+|p_1|}^{|\mathbf{p}|-|p_1|} \xi_{[p_2, \dots, p_m]}^{(k)} e^{i\omega(k+p_1)\tau} d\tau. \quad (\text{C.2})$$

This integral can be evaluated summand by summand. For  $k = -p_1$ , the exponential term in the integrand becomes 1, yielding the non-periodic, linear term

$$\int_0^t \xi_{[p_2, \dots, p_m]}^{(-p_1)} d\tau = t \xi_{[p_2, \dots, p_m]}^{(-p_1)}. \quad (\text{C.3})$$

Assume now that  $\xi_{[p_2, \dots, p_m]}^{(-p_1)}$  is nonzero. As  $p_1 = \sum_{l=1}^1 p_l \neq 0$ , by the induction assumption there must exist a  $w$  such that  $-p_1 = \sum_{l=2}^w p_l$ . But this is prohibited by construction of  $\mathbf{p}$  as it would imply  $\sum_{l=1}^w p_l = 0$ . We conclude that  $\xi_{[p_2, \dots, p_m]}^{(-p_1)}$  must be zero and  $\xi_{\mathbf{p}}(t)$  does not have a non-periodic term of the form (C.3).

For  $k \neq -p_1$ , the exponential term in the integrand does not disappear and we obtain

$$\int_0^t \xi_{[p_2, \dots, p_m]}^{(k)} e^{i\omega(k+p_1)\tau} d\tau = \frac{1}{i\omega(k+p_1)} \xi_{[p_2, \dots, p_m]}^{(k)} \left( e^{i\omega(k+p_1)t} - 1 \right). \quad (\text{C.4})$$

As (C.3) vanishes and all other summands are of the form (C.4), which is  $T$ -periodic,  $\xi_{\mathbf{p}}$  is again  $T$ -periodic. In particular, Equation (C.4) allows to read off the Fourier coefficients of  $\xi_{\mathbf{p}}$ :

$$\xi_{\mathbf{p}}^{(0)} = \sum_{k=-|\mathbf{p}|}^{|\mathbf{p}|} \frac{-1}{i\omega(k+p_1)} \xi_{[p_2, \dots, p_m]}^{(k)} \quad (\text{C.5a})$$

$$\xi_{\mathbf{p}}^{(k)} = \frac{1}{i\omega k} \xi_{[p_2, \dots, p_m]}^{(k-p_1)} \quad k \neq 0. \quad (\text{C.5b})$$

By the induction assumption,  $\xi_{\mathbf{p}}^{(k)}$  for  $k \neq 0$  can only be nonzero if there is a  $w$  such that  $k - p_1 = \sum_{l=2}^w p_l$ , which completes the proof.  $\square$

## References

- [1] M. Géradin, D. J. Rixen, Mechanical Vibrations. Theory and Application to Structural Dynamics, 3rd Edition, Wiley, New York, 2014.
- [2] T. F. Schubert, E. M. Kim, Fundamentals of Electronics: Book 4 Oscillators and Advanced Electronics Topics, Springer International Publishing, 2016. doi:10.1007/978-3-031-79886-3.
- [3] A. H. Nayfeh, B. Balachandran, Applied Nonlinear Dynamics, Wiley Series in Nonlinear Science, Wiley-VCH, Weinheim, 1995.
- [4] G. Teschl, Ordinary Differential Equations and Dynamical Systems, no. 140 in Graduate Studies in Mathematics, American Mathematical Society, Providence, Rhode Island, 2012.
- [5] G. Moore, Floquet theory as a computational tool, SIAM Journal on Numerical Analysis 42 (6) (2005) 2522–2568. doi:10.1137/s0036142903434175.
- [6] L. Peletan, S. Bagnuet, M. Torkhani, G. Jacquet-Richardet, A comparison of stability computational methods for periodic solution of nonlinear problems with application to rotordynamics, Nonlinear Dynamics 72 (3) (2013) 671–682. doi:10.1007/s11071-012-0744-0.



- [7] E. Hairer, S. P. Nørsett, G. Wanner, Solving Ordinary Differential Equations I: Nonstiff Problems, 2nd Edition, Springer, Berlin ; Heidelberg, 2008.
- [8] R. D. Skeel, Thirteen ways to estimate global error, *Numerische Mathematik* 48 (1) (1986) 1–20. doi:10.1007/bf01389440.
- [9] A. Lazarus, O. Thomas, A harmonic-based method for computing the stability of periodic solutions of dynamical systems, *Comptes Rendus Mécanique* 338 (9) (2010) 510–517. doi:10.1016/j.crme.2010.07.020.
- [10] T. Detroux, L. Renson, L. Masset, G. Kerschen, The harmonic balance method for bifurcation analysis of large-scale nonlinear mechanical systems, *Computer Methods in Applied Mechanics and Engineering* 296 (2015) 18–38. doi:10.1016/j.cma.2015.07.017.
- [11] J. Zhou, T. Hagiwara, M. Araki, Spectral characteristics and eigenvalues computation of the harmonic state operators in continuous-time periodic systems, *Systems & Control Letters* 53 (2) (2004) 141–155. doi:10.1016/j.sysconle.2004.03.002.
- [12] L. Guillot, A. Lazarus, O. Thomas, C. Vergez, B. Cochelin, A purely frequency based Floquet-Hill formulation for the efficient stability computation of periodic solutions of ordinary differential systems, *Journal of Computational Physics* 416 (2020) 109477. doi:10.1016/j.jcp.2020.109477.
- [13] F. Bayer, R. I. Leine, Sorting-free Hill-based stability analysis of periodic solutions through Koopman analysis, *Nonlinear Dynamics* 111 (9) (2023) 8439–8466. doi:10.1007/s11071-023-08247-7.
- [14] F. Bayer, R. I. Leine, O. Thomas, A. Grolet, Koopman-Hill stability computation of periodic orbits in polynomial dynamical systems using a real-valued quadratic harmonic balance formulation, *International Journal of Non-Linear Mechanics* 167 (2024) 104894. doi:10.2139/ssrn.4811433.
- [15] M. McGurk, J. Yuan, Prediction and validation of aeroelastic limit cycle oscillations using harmonic balance methods and Koopman operator, Preprint. (Jan. 2025). doi:10.21203/rs.3.rs-5859544/v1.
- [16] C. Chicone, *Ordinary Differential Equations with Applications*, 2nd Edition, Springer New York, 2006. doi:10.1007/0-387-35794-7.
- [17] E. Abboud, A. Grolet, H. Mahé, O. Thomas, Computation of dynamic transmission error for gear transmission systems using modal decomposition and Fourier series, *Forschung im Ingenieurwesen* 86 (4) (2021) 751–755. doi:10.1007/s10010-021-00571-x.
- [18] K. Moran, C. Burgner, S. Shaw, K. Turner, A review of parametric resonance in microelectromechanical systems, *Nonlinear Theory and Its Applications*, *IEICE* 4 (3) (2013) 198–224. doi:10.1587/nolta.4.198.
- [19] M. Ramírez-Barrios, F. Dohnal, Reduction of settling time by multi-frequency pulsed parametric excitation, *Nonlinear Dynamics* 112 (9) (2024) 7185–7198. doi:10.1007/s11071-024-09281-9.
- [20] B. O. Koopman, Hamiltonian systems and transformation in Hilbert space, *Proceedings of the National Academy of Sciences of the United States of America* 17 (16577368) (1931) 315–318. doi:10.1073/pnas.17.5.315.
- [21] A. Mauroy, I. Mezić, Global stability analysis using the eigenfunctions of the Koopman operator, *IEEE Transactions on Automatic Control* 61 (2016) 3356–3369. doi:10.1109/TAC.2016.2518918.
- [22] A. Mauroy, I. Mezić, Y. Susuki (Eds.), *The Koopman Operator in Systems and Control. Concepts, Methodologies and Applications*, no. 484 in *Lecture Notes in Control and Information Sciences*, Springer, Cham, 2020.
- [23] S. L. Brunton, M. Budišić, E. Kaiser, J. N. Kutz, Modern Koopman theory for dynamical systems, *SIAM Review* 64 (2) (2022) 229–340. doi:10.1137/21m1401243.
- [24] D. Bruder, X. Fu, R. B. Gillespie, C. D. Remy, R. Vasudevan, Data-driven control of soft robots using Koopman operator theory, *IEEE Transactions on Robotics* 37 (3) (2021) 948–961. doi:10.1109/TR0.2020.3038693.

- [25] M. Budišić, R. Mohr, I. Mezić, Applied Koopmanism, *Chaos: An Interdisciplinary Journal of Nonlinear Science* 22 (4) (2012) 047510. doi:10.1063/1.4772195.
- [26] K.-J. Engel, R. Nagel, One-parameter semigroups for linear evolution equations, [nachdr.] Edition, no. 194 in *Graduate Texts in Mathematics*, Springer, New York, 2008.
- [27] S. L. Brunton, B. W. Brunton, J. L. Proctor, J. N. Kutz, Koopman invariant subspaces and finite linear representations of nonlinear dynamical systems for control., *PLoS ONE* 11 (2) (2016) e0150171. doi:10.1371/journal.pone.0150171.  
URL <http://europepmc.org/articles/PMC4769143?pdf=render>
- [28] S. H. Son, H.-K. Choi, J. Moon, J. S.-I. Kwon, Hybrid Koopman model predictive control of nonlinear systems using multiple EDMD models: An application to a batch pulp digester with feed fluctuation, *Control Engineering Practice* 118 (2022) 104956. doi:10.1016/j.conengprac.2021.104956.  
URL <https://www.sciencedirect.com/science/article/pii/S09670666121002331>
- [29] Z. G. Nicolaou, G. Huo, Y. Chen, S. L. Brunton, J. N. Kutz, Data-driven discovery and extrapolation of parameterized pattern-forming dynamics, *Physical Review Research* 5 (4) (2023) 1042017. doi:10.1103/physrevresearch.5.1042017.
- [30] L. V. Ahlfors, *Complex Analysis*, 3rd Edition, *International Series in Pure and Applied Mathematics*, McGraw-Hill, New York [u.a.], 2007.
- [31] H. Broer, F. Takens, *Dynamical Systems and Chaos*, Springer New York, 2011. doi:10.1007/978-1-4419-6870-8.
- [32] C. Moler, C. Van Loan, Nineteen dubious ways to compute the exponential of a matrix, twenty-five years later, *SIAM Review* 45 (1) (2003) 3–49. doi:10.1137/S00361445024180.
- [33] A. H. Al-Mohy, N. J. Higham, A new scaling and squaring algorithm for the matrix exponential, *SIAM Journal on Matrix Analysis and Applications* 31 (3) (2009) 970–989. doi:10.1137/09074721x.
- [34] J. Ibáñez, J. M. Alonso, P. Alonso-Jordá, E. Defez, J. Sastre, Two Taylor algorithms for computing the action of the matrix exponential on a vector, *Algorithms* 15 (48) (2022). doi:10.3390/a15020048.
- [35] W. Feller, *An Introduction to Probability Theory and its Applications*, 3rd Edition, Vol. 1, Wiley, New York, NY, 1968.
- [36] M. Oberguggenberger, A. Ostermann, *Analysis for Computer Scientists: Foundations, Methods, and Algorithms*, Springer International Publishing, Cham, 2018. doi:10.1007/978-3-319-91155-7.